Published in final edited form as:
Adv Drug Deliv Rev. 2014 September 30; 0: 79–97. doi:10.1016/j.addr.2014.08.002.

Targeted Nanotechnology for Cancer Imaging

Randall Toy[1,2], **Lisa Bauer**[2,3], **Christopher Hoimes**[4,5], **Ketan B. Ghaghada**[6,7], and **Efstathios Karathanasis**[1,2,4,8,*]

[1]Department of Biomedical Engineering, Case Western Reserve University, Cleveland, Ohio 44106

[2]Case Center for Imaging Research, Case Western Reserve University, Cleveland, Ohio 44106

[3]Department of Physics, Case Western Reserve University, Cleveland, Ohio 44106

[4]Case Comprehensive Cancer Center, Case Western Reserve University, Cleveland, Ohio 44106

[5]University Hospitals Case Medical Center, Cleveland, Ohio 44106

[6]Edward B. Singleton Department of Pediatric Radiology, Texas Children's Hospital, Houston, Texas 77030

[7]Department of Radiology, Baylor College of Medicine, Houston, Texas 77030

[8]Department of Radiology, Case Western Reserve University, Cleveland, Ohio 44106

Abstract

Targeted nanoparticle imaging agents provide many benefits and new opportunities to facilitate accurate diagnosis of cancer and significantly impact patient outcome. Due to the highly engineerable nature of nanotechnology, targeted nanoparticles exhibit significant advantages including increased contrast sensitivity, binding avidity and targeting specificity. Considering the various nanoparticle designs and their adjustable ability to target a specific site and generate detectable signals, nanoparticles can be optimally designed in terms of biophysical interactions (*i.e.*, intravascular and interstitial transport) and biochemical interactions (*i.e.*, targeting avidity towards cancer-related biomarkers) for site-specific detection of very distinct microenvironments. This review seeks to illustrate that the design of a nanoparticle dictates its *in vivo* journey and targeting of hard-to-reach cancer sites, facilitating early and accurate diagnosis and interrogation of the most aggressive forms of cancer. We will report various targeted nanoparticles for cancer imaging using X-ray computed tomography, ultrasound, magnetic resonance imaging, nuclear imaging and optical imaging. Finally, to realize the full potential of targeted nanotechnology for cancer imaging, we will describe the challenges and opportunities for the clinical translation and widespread adaptation of targeted nanoparticles imaging agents.

*Author to whom correspondence should be addressed: Efstathios Karathanasis 2071 Martin Luther King Jr. Drive, Wickenden Building, Cleveland, Ohio 44106, USA Phone: +1-216.844.5281; Fax: +1-216.844.4987; stathis@case.edu.

NIH-PA Author Manuscript

NIH-PA Author Manuscript

Keywords

Targeted nanoparticles; cancer imaging; MRI; CT; ultrasound; PET; SPECT; optical imaging

1. Introduction

Due to the unique material properties that appear at the nanoscale, nanoparticles provide many benefits and new opportunities to address the complexity of cancer. Historically, attempts to improve nanoparticle homing to tumors have relied on the enhanced permeability and retention (EPR) effect to direct imaging and therapeutic agents to the primary site [1–10]. This stemmed from the success of liposomal anthracyclines, which were among the first, and to date the most extensively utilized, nano-therapeutics to be approved for clinical use. By exploiting the leaky vasculature of the tumor microenvironment [6], it was universally accepted that a 100-nm liposomes with polyethylene glycol (PEG) coating offered improved delivery of therapeutics to tumors while reducing off-target delivery [7–9]. Following the success stories of nanotherapeutics, nanoparticle contrast agents have been developed for a wide range of imaging modalities, which include Computed Tomography (CT), Magnetic Resonance Imaging (MRI), Positron Emission Tomography (PET), ultrasound and optical imaging.

However, current practice indicates that the benefit of nanoparticle imaging agents in a variety of targeting contexts has not yet reached its ultimate potential for translating to the clinic. This is related to the fact that nanoscientists initially adapted the nanoparticle-based therapeutic strategies for imaging applications. Shared advantages for nanoparticle-based therapeutic and imaging agents initially included prolonged blood circulation and the ability to load high concentrations of molecular agents. This was beneficial for the first generation nanoparticle imaging agents, which were primarily designed as blood pool agents. On the other hand, targeted nanoparticles and molecular imaging requires different design strategies. First, many recent publications, have started pointing out that the impact of the EPR effect is more heterogeneous than it was initially thought [11]. Second, the EPR effect is a prerequisite for receptor-mediated targeting of a nanoparticle to cancer cells in the deep interstitial space. However, in this case, the signal of the event (*i.e.* targeting of the cancer biomarker) will be difficult to discriminate from the non-specific signal generated due to the EPR-driven accumulation of the nanoparticle in cancerous tissues. Third, while prolonged blood residence of a nanoparticle may be advantageous for EPR-driven therapeutic strategies, it may be detrimental for targeted imaging applications. Since accurate detection requires sufficient signal difference between the lumen of the blood vessels and the targeting site, imaging may need to be delayed for days after injection to allow the agent to clear from the bloodstream.

Furthermore, to date, the preclinical development of nanoparticle systems has mainly focused on targeting primary tumors of relatively large sizes. These results obtained from mouse studies, however, are somewhat disconnected from clinical practice. A clinician would prefer to detect small lesions at an early stage, when therapeutic interventions are most effective. While the EPR effect may be effective in well-vascularized tumors of several millimeters in diameter [2], it is ineffective in the early development of primary tumors or micrometastatic disease, which presents small clusters of malignant cells within variable tissue types [12, 13]. For example, meta-analysis has shown that current clinical modalities (*e.g.* CT, MRI, FDG PET) can detect large metastatic tumors (>1 cm) with high accuracy [14–16]. However, by the time metastatic disease becomes clinically evident, long-term patient outcomes are not favorable [17]. Unfortunately, current imaging rarely detects the early stages of cancer development at the primary or metastatic site (*i.e.* the early spread of tumor cells) [18], which prohibits early and effective interventions [19]. Apparently, targeting an occult lesion hidden within a large population of normal cells presents a unique challenge.

However, in the last decade, nanoscientists have recognized that nanoparticle technology exhibits a highly engineerable nature, which is governed by its own distinctive principles in terms of targeting interactions with cells and intravascular, transvascular and interstitial transport. While conventional small molecular agents are rapidly distributed within cancer and healthy tissues in a non-specific manner, targeted nanoparticles can be optimally designed in terms of biophysical interactions (*i.e.* intravascular and interstitial transport) and biochemical interactions (*i.e.* targeting avidity towards cancer-related biomarkers) for site-specific navigation within a very distinctive microenvironment. Once one considers the various nanoparticle designs and their adjustable ability to target a specific site and generate detectable signals, many questions arise. What should be the nanoparticle's material, size, shape and polymer coating? How long should the nanoparticle circulate? Which types of targeting ligands and how many of them should a nanoparticle have? What is the safe dose of the agent and how is that compared to the dose required to accomplish detection? How will detection of a specific cancer microenvironment impact the decision-making process of the oncologist?

This review illustrates that the design of a nanoparticle dictates its *in vivo* journey and ultimately targeting of hard-to-reach cancer sites, which facilitates the early and accurate diagnosis and interrogation of the most aggressive forms of cancer. In the proceeding sections, we will discuss how the design of nanoparticles should be tailored to improve targeting, examine targeted nanoparticles under preclinical development, and evaluate how we can expedite the translation of nanoparticle imaging agents. First, the physiological obstacles to nanoparticle targeting will be discussed. Next, we will evaluate how a nanoparticle's size, shape, and surface chemistry can be selected to increase targeting to tumors. More specifically, we will discuss how to design nanoparticles both for deep interstitial targeting and vascular targeting. After this discussion, we will review nanoparticle imaging agents designed for x-ray computed tomography (CT), ultrasound, magnetic resonance imaging (MRI), positron emission tomography (PET), single photon emission computed tomography (SPECT) and optical imaging. We will conclude by describing challenges and opportunities for the clinical translation of targeted nanotechnology for imaging.

2. Obstacles to the Widespread Use of Nanoparticle Imaging Agents for Cancer

While abundant in preclinical development, nanoparticles are rarely used in the clinic. Since an unmet clinical need today is the detection of early tumor development at primary and metastatic sites, nanoparticles can be widely adopted in the clinic due to their potential of targeting accuracy to tumors. Certainly, the design of imaging methodologies that could detect tumors earlier would significantly improve patient outcomes. For example, the early detection of breast cancer has been shown to improve 5-year survival from 23% for distant-stage breast cancer to 84% for regional stage breast cancer [20]. Historically, the primary mode of targeting nanoparticles to tumors is the EPR effect. In essence, this mechanism is the passive extravasation of nanoparticles from the tumor microcirculation to the tumor interstitial space [21–23]. Unlike healthy vasculature, tumor neovasculature is characterized by a discontinuous vascular endothelium. The rate of tumor angiogenesis results in the formation of gaps, ranging between 100–1000 nm in width (depending on tumor type) between pericytes and smooth muscle cells, which permit the passage of nanoparticles (Fig. 1) [24–28]. As we discuss in section 3.1, unfortunately, this extravascular transport of nanoparticles is inconsistent throughout a tumor [22, 24, 29–32]. As a result, nanoparticle imaging agents may fail to highlight the entire tumor, which leads to an underestimation of tumor proliferation. Furthermore, the microenvironment of a primary tumor is often very different than that of an early metastatic site. Prior to initiation of the angiogenic switch, which leads to rapid blood vessel development and tumor exponential growth, the blood vessels in the proximity of early metastasis remain intact. While the field of nanotechnology has historically exploited the EPR effect to target tumors at the primary site, targeting circulating tumor cells (CTCs) or micrometastases cannot rely on the use of passive mechanisms to deliver nanoparticles to tumors [12]. To design targeted nanoparticle imaging agents with both high diagnostic sensitivity and specificity, new methods must be devised based on active targeting schemes considering the microenvironment of the target site (*e.g.*, the type of cancer, its location and stage). Depending on whether a nanoparticle seeks a vascular, a deep tissue or a blood-circulating target, the design of a nanoparticle requires different considerations and features. For example, ligand-functionalized magnetic iron oxide nanoparticles can bind to CTCs, which can be captured using immunomagnetic separation [33, 34]. In the case targeting metastasis, vascular targeting may be more effective than deep tissue targeting (which requires the EPR effect). Thus, the design of a nanoparticle imaging agent, which seeks and binds to overexpressed receptors on the blood vessels that supply metastatic lesions, should be different than a nanoparticle that is purposed for deep interstitial targeting. For a vascular targeting strategy to be effective, since extravasation is not required, it is critical to design nanoparticles, which have a tendency to travel to the blood vessel wall and target vascular markers with high binding avidity, considering the high shear forces resulting from blood flow. Both vascular and deep tissue targeting approaches will be discussed at length in this review.

3. Engineering Targeted Nanoparticles for Cancer Imaging

In order to maximize the diagnostic accuracy of a nanoparticle imaging agent, it is essential to design it in a manner, which maximizes its transport to a cancerous lesion. Fortunately, design flexibility is the major advantage of targeted nanoparticle technology. A wealth of materials, which include lipids, metals, and polymers, enable the production of nanoparticles for many clinical imaging modalities (*e.g.* CT, MRI, and ultrasound) (Fig. 2). Top-down nanofabrication approaches, such as the particle replication in non-wetting templates (PRINT) method and the dip-pen nanolithography method, produce nanoparticles with a wide variety of sizes, shapes and structures from a variety of different materials [36, 37]. These shapes range in complexity from spheres, rods, and cubes to structures resembling snowflakes, flowers, thorns, hemispheres, worms, discoids, and chains [38]. In addition, there is an abundance of chemistries that enables the conjugation of polymers and ligands to nanoparticles, which improve biocompatibility and targeting specificity. To be approved by the FDA, nanoparticles must undergo rigorous pre-clinical testing and validation, which include safety and toxicity studies. In comparison to nanoparticle therapeutics, consideration of safety is even more important with nanoparticle imaging agents, since these could be administered to healthy individuals.

With the flexibility to manufacture nanoparticles of different sizes, shapes, and materials, nanoparticle design can be optimized to maximize the sensitivity and specificity of tumor targeting. By fine-tuning a nanoparticle's size, shape, and surface chemistry, its margination and targeting abilities can be dramatically improved. Margination, the ability of a nanoparticle to escape the blood flow and move to the vessel wall, is a required process to target a nanoparticle to a tumor. If a nanoparticle's radial movement in a blood vessel is limited, the opportunity for binding interactions between the nanoparticle and the vessel wall will also be restricted. Modification of a nanoparticle's size, shape, and surface chemistry also affects its binding avidity and internalization. An ideal nanoparticle contrast agent for tumor targeting would be produced with the following characteristics: 1) high rate of margination, 2) strong binding avidity to tumor sites, and 3) rapid internalization by the targeted cells. Creating a nanoparticle with all three of these characteristics is challenging; this is because modification of one nanoparticle design parameter may enhance one or more of these characteristics at the expense of one of the others (Table 1). In this context, targeted nanoparticle imaging agents must be designed with consideration of all of these biochemical and biophysical phenomena. Nanoparticle targeting performance is traditionally evaluated through independent *in vitro* internalization, *in vivo* pharmacokinetics, and biodistribution studies. A caveat with the majority of *in vitro* internalization studies is that they often neglect the effect of flow on nanoparticle transport to the vessel wall. More accurate assessment of *in vitro* nanoparticle targeting can be done in parallel plate chambers and microfluidic setups, which replicate vascular morphology and allow for the control of local flow [39–41]. Similarly, nanoparticle *in vivo* studies primarily focus on the efficacy of polymers that extend circulation half-life and targeting ligands that improve tumor specificity without consideration of hemodynamics or the uniqueness of different tumor microenvironments. Not only do these studies neglect the importance of nanoparticle geometry, they fail to take into account variability in fluid dynamics, which has been shown

NIH-PA Author Manuscript

NIH-PA Author Manuscript

to be one of the primary obstacles to nanoparticle delivery to tumors. In this section, we will provide examples of how the size of PEGylated liposomes or the shape of gold or iron oxide nanoparticles dictate tumor targeting in both deep tissue and vascular targeting strategies. However, it is important to appreciate that extraction of general rules is very challenging, since the *in vivo* behavior of nanoparticles depends on both the tumor model (*e.g.*, mouse strain, tumor type, location and stage of tumor) and the characteristics of the nanoparticle (*e.g.*, type of nanoparticle, polymer coating, surface charge). By using these specific examples, our intention is to illustrate that rational design of a nanoparticles can lead to significantly improved imaging of cancer.

3.1 Deep tissue targeting

3.1.1 Intravascular and transvascular transport of nanoparticles—To maximize nanoparticle imaging agent accumulation and tumor detection accuracy, it is essential to consider nanoparticle size, shape, and surface chemistry as design parameters. These characteristics of nanoparticles have been shown to play a central role in their transport in tumor microcirculation [55]. Successful delivery of nanoparticles requires that the particle enters the tumor microcirculation, navigates through the tumor leaky vasculature into the tumor interstitium (extravasation step) and is delivered to cytoplasmic targets in cancer cells. However, nanoparticles *en route* to their target face numerous biobarriers created by the tumor abnormal physiology. Abnormal tumor features, including physically compromised vasculature, erratic blood flow, abnormal extracellular matrix, and high interstitial fluid pressure, can limit the effective delivery of nanoparticles into tumors. Due to these biobarriers, extravasation of nanoparticles is often inconsistent throughout a tumor [22, 24, 29–32, 62–64].

The first efforts to increase the extravasation rates were focused on prolonging the blood circulation of nanoparticles. Numerous studies have shown that a long circulating nanoparticle has more opportunities to pass through the tumor vasculature, which increases its chances of accumulation at the tumor site [6, 65–69]. Nanoparticle size was the first design parameter that was studied in relation to blood circulation and its effect on extravasation. In general, particles less than 5–10 nm are cleared from the circulation through renal clearance [42]. As particle size increases, nanoparticle accumulation primarily occurs in the liver and spleen [43]. For example, liposomes being the first nanoparticle system to be extensively studied, it was identified that a PEGylated liposome with a diameter between 60–100 nm (hydrodynamic size) maximizes blood residence time [44, 45, 70]. In another case of a solid nanoparticle, from a library of PEGylated gold nanoparticles with sizes between 20–90 nm, a maximum blood circulation was also observed for particles with a size of approximately 60 nm [71].

Regarding the variable extravasation patterns of the same nanoparticle among different tumors, it was initially recognized that the most likely contributor is the physical gaps of the tumor's leaky endothelium [21, 22, 27, 72]. In addition to the microvascular architecture [24–28], this variability in nanoparticle deposition is also due to the effect of blood flow on the transport of a nanoparticle. Unlike small molecules, which move primarily by diffusion, nanoparticle movement is influenced by convection and to a lesser degree by diffusion [73–

75]. As a result, the blood flow in a tumor critically influences nanoparticle deposition [76–78]. This is important because variability in blood flow is high in tumors depending on the tumor vessel's tortuosity, diameter, and vascular permeability [79, 80]. Furthermore, high interstitial pressure counters blood flow, resulting in a net movement of nanoparticles away from the interstitial space [81]. Thus, the success of deep tissue targeting of nanoparticle imaging agents is directly linked to the variability of blood flow within a tumor. For nanoparticles to overcome interstitial pressure, high blood flow is necessary to push nanoparticles into the interstitial space. Tumors, however, are known to have blood flow profiles with regions of both low and high flow. The effect of flow on nanoparticle accumulation has been verified experimentally. In tumor spheroids, an increase in blood flow from 800 to 7000 mL/min resulted in a two-fold increase in the deposition of PEGylated gold nanoparticles with a hydrodynamic diameter of 40 nm [82]. Another study found that a nanoparticle's size dictates the extent to which blood flow affects its transport. A threefold increase in blood flow resulted in a 100-fold elevated intratumoral deposition of PEGylated liposomes with a hydrodynamic diameter of 100 nm [30] (Fig. 3). On the contrary, the same increase in blood flow enhanced the deposition of smaller PEGylated liposomes (~30 nm) by less than an order of magnitude. While the contribution of diffusion on nanoparticles transport is much smaller than convective forces, these differences can be explained by the higher effect of convection on the transport of larger nanoparticles and the larger effect of diffusive transport on the transport of smaller nanoparticles. Because diffusive motion is random, nanoparticles moving by diffusion can move in and out of a tumor interstitium with similar ease. Therefore, smaller nanoparticles have a higher rate of washout from the tumor than bigger nanoparticles. For example, EGFR-targeted and non-targeted 100-nm liposomes had similar levels of intratumoral accumulation at any blood flow. While EGFR-targeted 30-nm liposomes increased their intratumoral accumulation by 10-fold in comparison to their non-targeted counterparts at low blood flows, targeting did not significantly increase the 30-nm liposome's accumulation at high blood flows. At high blood flow, convection was sufficient to retain the small liposomes in the tumor even in the absence of targeting. In section 4, we will show examples demonstrating the importance of nanoparticle's size for effective deep tissue targeting and its relation to cancer imaging and detectability.

Due to the *in vivo* complexity of deep tissue targeting of tumors, we typically cannot separately study the individual transport processes of nanoparticles in tumor models in rodents. Such studies, however, can be performed *in vitro* in a controlled manner using parallel plate chambers and microfluidic setups, which replicate vascular morphology and allow for the control of local flow [39–41]. Prior to extravasation, one of the pivotal steps dictating the intratumoral fate of nanoparticles is their margination (i.e. lateral drift) towards the blood vessel walls. Near-the-wall margination is not just desirable; it is required for the particle to be able to interact with the tumor vascular bed. Subsequently, the particle will have the chance to either target tumor-specific vascular biomarkers or extravasate through the tumor leaky endothelium into the tumor interstitium. Even though tumors display blood flows significantly slower than that of normal circulation, nanoparticles, due to their size, are primarily transported in the tumor microcirculation *via* convective means and therefore margination is not favored. In order for a particle to escape the blood flow streamlines resulting in margination, forces that depend on the particle characteristics such as gravity, buoyancy, diffusion or torque are required [83, 84]. Apparently, only the latter two factors are important for nanoparticle margination [85, 86]. For example, *in vitro* flow studies in microfluidic devices showed that the margination of a PEGylated liposome with a hydrodynamic size of 60 nm was significantly higher than that of a 100-nm liposome [39]. This finding can be attributed to the higher effect of convection on the transport of larger nanoparticles, which have difficulty escaping the blood flow. In contrast, smaller nanoparticles that rely relatively more on diffusive transport are able to marginate towards the vessel walls more effectively.

Furthermore, the shape of a nanoparticle imaging agent also affects its intravascular and transvascular transport. In the case of nanoparticle margination in microcirculation, because hydrodynamic forces dictate the transport of nanoparticles, symmetrical and asymmetrical particles have different trajectories when travelling through a blood vessel (Fig. 4). A symmetrical nanoparticle, such as a sphere, has the same distribution of forces acting on it regardless of its angular orientation. As a result, symmetrical nanoparticles tend to remain in the center of the blood vessel while traveling through circulation. In contrast, variable drag forces and torques act on asymmetric nanoparticles, such as rods or discs, as they are moved by flow [52]. These forces results in a tumbling motion that leads to increased nanoparticle drift towards the vessel wall [53, 54]. Three distinct classes of nanoparticles of different shapes - discoidal (AR: 0.5), hemispherical, and ellipsoidal (AR:0.5) displayed increased margination behavior in comparison to spheres [55]. More quantitatively, a PEGylated gold nanorod was observed to marginate 7 times more than a PEGylated gold nanosphere of an equivalent diameter in a straight microchannel at a physiological flow rate (50 μL/min) [39]. At that same flow rate, a flexible PEGylated iron oxide nanochain (20 × 100 nm; hydrodynamic size) was observed to marginate 5 times more than an iron oxide nanosphere (20 nm) [56]. These differences in margination behavior strongly motivate the tailoring of shape to improve the vascular targeting of nanoparticle imaging agents as we will discuss in section 3.2.

Furthermore, it has been found that nanoparticle asymmetry also increases binding avidity. Comparison of the binding avidity of nanoparticles of different shapes can be achieved through calculation of the active fractional area of the nanoparticle (AFAC) [61]. The AFAC parameter takes into consideration not only the particle's shape, but also the length and flexibility of the polymer, which displays the particle's targeting ligands (Fig. 5). With polymer surface density, length, and flexibility held constant, the AFAC of a rod is higher than the AFAC of a sphere. Therefore, a nanoparticle's shape has direct ramifications on its binding avidity. In agreement with these theoretical calculations, targeted nanorods have been observed to localize at the target site seven times more than their targeted spherical counterparts [58].

3.1.2 Effect of ligand density—Increasing the surface density of the targeting ligand strongly affects the nanoparticle's rate of cellular uptake. Receptors are frequently expressed in unique, clustered distributions that depend on the receptor type and cell type. By increasing the surface density of ligands on the nanoparticle, there is a higher chance of nanoparticle association with the receptor clusters. For example, increasing the density of

HER2-targeting ligands on liposomes from 1 to 2% resulted in a doubling of uptake by BT-474 cells [60]. When the ligand density was further increased from 2% to 3%, however, only a 10% increase in BR-474 cellular uptake was observed [60]. This suggests that excessive functionalization of a nanoparticle's surface may not necessarily lead to an improvement in tumor targeting. Thus, the use of a high number of ligands could actually be detrimental. The relation of cell uptake to the nanoparticle's ligand density follows a typical bell-shaped pattern [87]. For example, the uptake of PSMA-targeted PLGA-PEG nanoparticles increased as the PEG density increased to 14 mol% [59]. Above this threshold for this specific nanoparticle design, nanoparticle uptake by cancer cells started decreasing. It is likely that at very high ligand densities, a nanoparticle's immunogenicity increases. More importantly, the higher ligand density will saturate the receptor quickly, which will lead to fewer nanoparticles being internalized into the targeted cancer cells.

3.2 Vascular targeting

The approach to design nanoparticles imaging agents for deep tissue targeting that identify cancer cell receptors in the tumor interstitium is only viable if the tumor has an abundance of hyperpermeable vasculature. Unfortunately, early tumor development at primary or metastatic site lacks leaky vasculature until it is well developed and difficult to treat. For example, micrometastatic lesions (*i.e.* the early spread of cancer cells) are difficult to target because they lack leaky vasculature for targeting by passive mechanisms. It is highly desirable, however, to catch the early development of cancer (*i.e*., less than a few millimeters in diameter), because early therapeutic interventions are much more effective against early stage tumors. Without routes to gain entry into the tumor interstitium, vascular targeting appears as a more suitable strategy. For instance, micrometastatic sites overexpress an abundance of receptors that are typically not found in healthy tissue. In the metastatic niche, selectins (*e.g.* p-selectin, e-selectin) and other adhesion molecules (*e.g.* iCAM1, vCAM1, $\alpha_v\beta_3$ integrin) are overexpressed on the vessel wall [88, 89], which have been validated as targets for nanoparticle imaging agents [56, 90, 91]. With established targets, the next step would be to design optimized nanoparticles for different imaging modalities with high sensitivity to small metastatic lesions. As discussed, lesion size is inversely related to patient prognosis.

There are several ways to enhance the vascular targeting of nanoparticle imaging agent and accuracy for early detection of small lesions. As we discussed in section 3.1.1, designing a nanoparticle with asymmetry will enhance its margination, which is essential for the nanoparticle to interact with the vessel wall receptors. The use of an oblate-shaped nanoparticle, which has a higher AFAC, can also enhance binding avidity. For example, a chain-shaped iron oxide nanoparticle targeted to the $\alpha_v\beta_3$ integrin bound with 2.9 fold higher avidity than a spherical counterpart targeted to the same receptor in a microfluidic channel [56]. *In vivo*, vascular targeting of the iron oxide nanochain to the $\alpha_v\beta_3$ integrin resulted in a tenfold higher deposition at the site of a metastasis than its spherical counterparts [92]. The flexibility of the nanochain is also thought to improve its ability to bind to the vascular bed. Ligand density, dependent on the size and shape of the nanoparticle, is also a critical parameter to optimize. In the blood vessel, this is extremely important because the nanoparticle will have to battle shear forces that could potentially lead to particle detachment from the receptor site. The next section will evaluate a variety of targeted nanoparticles that have been already developed for the imaging modalities of computed tomography, ultrasound, MRI, nuclear imaging, and optical imaging, using targets both in the tumor interstitium and on the vascular bed.

4. Targeted Nanoparticle Imaging Agents

Targeted nanoparticle imaging agents provide a new paradigm in cancer imaging, one that goes beyond anatomical characterization, which enables early detection of cancer as well as treatment monitoring at the molecular/cellular level. Unlike targeted molecular agents, nanoparticles facilitate the association of hundreds of thousands of imaging moiety per construct, enabling up to million-fold signal amplification. From a development perspective, targeted nanoparticle agents for use in cancer imaging can be sub-divided into two categories: vascular targeting agents and cancer cell (or deep tissue) targeting agents. Furthermore, targeted agents based on different nanoparticle platforms have been developed for use with several imaging modalities (Table 2).

4.1. Targeted nanoparticles for different imaging modalities

A wide variety of modalities are utilized for cancer imaging in the pre-clinical and clinical domain. X-ray imaging, including computed tomography, mammography and tomosynthesis, is one of the most commonly used imaging modality in the clinic. The technology is highly matured, enables rapid imaging (scan times less than a minute) and provides high spatial resolution. Due to its ubiquitous nature and low cost, CT imaging is often the primary modality of choice for use in a majority of cancer imaging procedures. However, the technique suffers from inherent low soft tissue contrast, relatively low contrast sensitivity (~mM range) and exposure to x-ray radiation. Advances in scanner hardware and image processing are bringing about paradigm shifts in reducing radiation exposure as well evolution of new techniques. These new developments are likely to expand the horizons of X-ray techniques, including in the field of molecular imaging. Nuclear imaging techniques, including positron emission tomography (PET) and single-photon emission computed tomography (SPECT), play an important role in cancer imaging, especially in cancer staging and treatment follow-up. The technique provides high contrast sensitivity (~nM range) and has been at the forefront for development and clinical implementation of novel molecular imaging probes; however, it suffers from relatively poor spatial resolution (~3–10 mm). In comparison to CT imaging, the availability of nuclear imaging systems is limited and the procedures are relatively expensive; primarily due to limited availability and cost for producing radioisotope agents. MRI provides excellent soft tissue contrast and relatively high spatial resolution. Despite its high clinical utilization for cancer diagnosis and monitoring, it is limited to tumors that are about 1cm^3 or bigger [150]. However, several new imaging methods and techniques are on the horizon for further expanding and enhancing the clinical utility of MRI [151–153]. These developments will likely impact and warrant the development of novel molecular imaging probes for translation into the clinic. Ultrasound imaging uses high-frequency sound waves for visualization of subcutaneous body structures. Despite its low cost, the use of US in cancer imaging has been limited due to low depth penetration and dependence on user performance. Optical imaging has been extensively used in the pre-clinical cancer arena. The technique, although limited to subcutaneous regions, provides high spatial resolution and excellent contrast sensitivity. Photo-acoustic imaging (PAI) is rapidly gaining interest and, in conjunction with novel imaging probes, enables sensitive and specific detection of superficial cancer as well as in intra-operative procedures.

4.1.1 Targeted CT Agents—While nanoparticle CT agents are excellent blood pool agents [30, 154], the development of targeted CT probes has been limited due to the low contrast sensitivity of the X-ray imaging technique. The majority of targeted CT probe development has been pursued using metal-based nanoparticles due to their high atomic weight and therefore increased X-ray attenuation compared to the conventional iodine moiety. Gold, bismuth, tantalum, ytterbium have been studied as potential elements for development of CT imaging agents. Due to receptor-mediated endocytosis of the associated imaging moiety, targeted agents can facilitate delivery of large payload within cancer cells. For example, imaging of solid tumors using targeted gold nanorods achieved a 5-fold increase in signal attenuation when compared to non-targeted nanorods [98].

As we mentioned in section 3.4, the nanoparticle size plays a key role in deep tissue targeting. To enable deep tissue penetration, smaller sized gold nanoparticles have been utilized to image a variety of surface markers overexpressed on cancer cells. HER2-targeted gold nanoparticles have shown improvement in detection of small tumors (~1.5 mm) in comparison to passive targeting [93, 96]. Compared to non-targeted 30-nm gold nanoparticles, their EGFR-targeted counterparts demonstrated improved contrast enhancement of relatively small tumors (4–5 mm) in a head and neck squamous cell carcinoma mouse model [95]. In general, targeted gold nanoparticles for CT imaging have been explored in a variety of targeting schemes, including prostate-specific membrane antigen (prostate tumors) [97], folate receptor (various types of cancer) [99], CD4 receptor (peripheral lymph nodes) [94] and low-density lipoprotein (LDL) receptor [155, 156].

As we already mentioned, bismuth also strongly attenuates X-rays. 30-nm bismuth-sulfide nanoparticles conjugated to LyP-1 homing peptide were developed for imaging breast tumors [100]. CT imaging at 24 h after injection demonstrated that the targeted agent resulted in ~ 2.5-fold higher tumor signal when compared to its non-targeted counterpart. In good agreement with the design rules discussed in section 3.4, this is an example of selection of the appropriate nanoparticle size that benefits from active targeting. Use of the targeted contrast agent enabled discrimination of signals between deep tissue targeting and nanoparticle accumulation solely driven by EPR. In contrast to larger nanoparticles (*e.g.* >50 nm), the retention of the targeted 30-nm nanoparticles in the tumor interstitium is much higher than their non-targeted counterparts, which have a high likelihood of returning back to the bloodstream.

Upconversion nanoparticles (UCNP) have also attracted significant attention for use in X-ray/multimodality imaging [157]. These are generally lanthanide doped rare-earth nanoparticles (such as Gd-, Yb- and Lu-doped) having intrinsic upconversion luminescence properties. For instance, multifunctional PEGylated $BaGdF_5$:Yb/Er nanoparticles have been developed as efficient UCNPs for use in MRI, CT and optimal imaging [158]. Targeted

UCNPs containing folic acid ligand have also been investigated for use as multi-modality molecular imaging probes [159]. In addition to their use as imaging agents, UCNPs efficiently ability near-IR light, facilitating the development of NIR-triggered theranostic agents for imaging and treatment of solid tumors [160–162]

An important new development in X-ray imaging is the advancement of spectral CT for decomposition of X-ray attenuating signatures (*i.e.* elemental decomposition), which overcomes potential signal interference from other high attenuating structures. For example, fibrin-targeted bismuth nano-colloids have been developed for imaging of blood clots in a rabbit model [101]. Spectral CT enables the superior visualization of clots by separating attenuation effects from bone. This spectral CT approach for elemental decomposition has also been demonstrated using fibrin-targeted lipid-encapsulated ytterbium nano-colloids [163]. In addition to gold and bismuth, CT nanoparticle agents have been developed based on tantalum [164]. While this novel class of solid metallic nanoparticles may open a window for the development of molecular CT agents, concerns surrounding their biodistribution, clearance, *in vivo* safety, and *in vivo* toxicity need to be investigated before pursuit of clinical translation.

To date, all of the clinically approved X-ray contrast agents are based on iodine as the imaging moiety. However, there is an increasing interest in identifying new elements (as well as molecular and nanoparticulate constructs) that can serve as highly sensitive X-ray imaging agents. However, the energy range of the various types of x-ray-based devices has to be carefully considered. For example, under the operating energies of a clinical mammography unit, bismuth can provide much higher contrast enhancement than iodine. By weighing the linear attenuation coefficients of an element with respect to the x-ray source energy spectrum, bismuth has a unique property in the 5–50 keV energy range. For example, the x-ray linear attenuation coefficient is 5–10 times higher in the 5–30 keV range than the 32–40 keV range. Similar to bismuth, gold provides a much higher contrast enhancement than iodine in the energy range of a mammography unit. Since small animal micro-CT scanners and mammography systems operate also at relatively low energy, bismuth and gold nanoparticles provide higher contrast enhancement than iodine. However, this is not the case with clinical CT scanners, which operate at much higher energies. Overall, high atomic weight elements, such as gadolinium, gold, bismuth, tantalum, ytterbium, are all excellent candidates for development of novel nano-probes with strong X-ray attenuating properties. In addition, these elements may also enable development of probes that facilitate treatment prognostication and monitoring, an area of unmet clinical need in the application space of X-ray contrast agents. However, concerns surrounding their biodistribution, clearance, in vivo safety, and in vivo toxicity should be incorporated into the pre-clinical research and development objectives of next generation novel CT contrast agents before pursuing clinical translation. Similarly, the development of multi-modality agents, as attractive as it may seem, also needs to be thoroughly assessed from the practicality of clinical implementation and regulatory challenges.

In the context of clinical translation, CT imaging exhibits many advantages, which include the wide availability of scanners, low cost and quick scanning times, precise quantification of signal, and the highest spatial resolution amongst all clinical modalities. Regardless of these advantages, targeted nanoparticles for CT imaging should be very carefully selected taking under consideration the appropriateness of the target site. To compensate for the inherent low contrast sensitivity and increase the likelihood of sensitive imaging with CT, such target sites should be of relatively large size and express high numbers of the targeting biomarker. In these cases, accumulation of large amounts of the agent may be achieved, which generates sufficient (and detectable) signal. The developments in X-ray hardware are rapidly advancing and therefore the opportunities and need for molecular imaging CT contrast agents is clearly on the horizon.

4.1.2 Targeted Ultrasound Agents—Although imaging of some organs with ultrasound (US) is challenging (*e.g.* lungs), US exhibits excellent spatial resolution and contrast sensitivity. While there have been recent examples of US agents at the nanoscale [165, 166], we will primarily report examples of targeted submicron- and micro-sized agents. Due to the short *in vivo* half-life of US agents, the vast majority of targeted agent development has focused on seeking vascular markers of tumor angiogenesis [105]. For example, using an RGD ligand or the anti-$\alpha_v\beta_3$ antibody LM609, targeted microbubbles produced a ~13- or 10-fold higher echo amplitude, respectively, compared to non-targeted control microbubbles [102, 103]. Furthermore, various peptides have been used as ligands to direct microbubbles to integrins associated with tumor vasculature [104, 106, 107]. In addition to integrins, targeted microbubbles have been used for imaging and monitoring VEGFR-2 expression during anti-angiogenic treatment [108, 167]. As we will discuss in section 4.3, this use of nanoparticle imaging agents facilitates rapid monitoring of treatment efficacy, which can result in more efficient ways to manage patient therapy.

Dual-targeting US agents for simultaneous imaging of two vascular biomarkers, VEGFR-2 and $\alpha_v\beta_3$, have also been evaluated [109]. Due to their higher avidity that comes from the multi-ligand approach, the dual-targeting US microbubble generated significantly higher signal compared to the single-targeting counterparts (Fig. 6). The benefits of multi-targeting strategies is consistent with previous reports of drug-loaded liposomes targeted to multiple receptors on tumor cells [168].

4.1.3 Targeted MRI Agents—A considerable amount of work has been done in the development and preclinical validation of targeted MRI nanoparticles. Superparamagnetic iron oxide (SPIO) nanoparticles are an attractive platform with the advantages of high micromolar detection thresholds, high T2* sensitivity, and the versatility to present a wide variety of ligands for cellular and molecular imaging [169]. The efficacy of iron oxide particles is governed by their magnetic properties that in turn are determined by their composition, size and morphology. To determine the optimal design parameters for SPIO nanoparticles, studies have been conducted to understand the effect of particle shape and size on the particle's magnetism and relaxivity [170, 171]. Vascular targeting of SPIO agents to integrins [110] or VEGFR [114] has been exploited for imaging of tumor-associated vasculature. Deep tissue targeting with SPIOs has also been explored to image primary tumors using targets such as urokinase plaminogen activator (uPA) [111, 112], transferrin receptors [115], HER2 receptors [172], chemokine receptor 4 [113].

Similar to T2 agents (*i.e.* SPIO), T1 nanoparticle agents have been developed based on gadolinium (Gd). Using lipid-based nanoparticles (*e.g.* liposomes, perfluorocarbon-based lipid nanoemulsions), targeted Gd-based liposomal agents have been extensively studied for vascular targeting of tumor angiogenesis (and inflammation) [124, 173], including ICAM-1 [121], $\alpha_v\beta_3$ integrin *in vivo* [117, 125, 126], VCAM-1 [174] and CD105 [122]. In comparison to conventional agents based on small molecules, liposomal agents enable attachment of thousands of Gd moieties per nanoparticle, which increases relaxivity by orders of magnitude on a nanoparticle basis [175]. Similar to US agents, dual-targeted Gd-based liposomes have been explored to further increase targeting specificity [119, 120]. However, contrary to *in vitro* results, the dual-targeted liposome did not produce an enhanced signal over RGD-targeted liposomes alone. Since the size of the liposomes was relatively large (*i.e.* >50nm), the lack of significance in the differences between the two constructs could very likely be due to a substantial component of signal arising from the non-specific tumor uptake (*e.g.* EPR effect), masking the signal from vascular targeting. Dendrimers are another attractive nanoparticle platform for Gd loading because of their narrow size distribution (~5–10 nm), branched structure, which facilitates the presentation of multiple ligands or contrast agents, and associated renal clearance. For example, Gd-loaded dendrimers targeting the folate receptor displayed enhanced MR signal in an animal model of KB tumor [129]. When designing Gd-based agents, several factors need to be considered since signal intensity at the target site is not linearly related to the concentration of the imaging moiety. For instance, the intracellular accumulation of Gd can markedly impact signal intensity [176]. Furthermore, the presentation of Gd atoms in a nanoparticle structure also impacts the efficiency of nanoparticle MR probes [175, 177, 178].

There is also potential for “activatable” contrast, wherein a targeted agent, composed of an iron oxide core surrounded by a polymer coating containing Gd-DTPA, quenches T1 contrast upon injection, but once exposed to an acidic environment such as a cancer cell lysosome, releases Gd-DTPA and generates T1 enhancement [179]. In addition, the flexibility in coating iron oxide cores with different functionalized polymeric materials has also facilitated the development of multimodal imaging agents. For instance, optical-MR agents have been developed by entrapping SPIOs within cRGD-targeted lipid particles labeled by fluorescent agents [116]. Besides T1 and T2 agents, nanoparticles, particularly liposomes, enabled the development of highly sensitive chemical exchange saturation transfer (CEST) agents, commonly referred as lipoCEST agents [180, 181]. CEST-MRI exploits the ability to resolve signal arising from protons on different molecules using controlled radiofrequency pulses [182]. By exploiting the slow transport of water protons through the lipid bilayer, the encapsulation of small molecule CEST agents in liposomes increases contrast sensitivity by three to four orders of magnitude. Vascular-targeted lipoCEST agents may be used to image brain tumor angiogenesis [127]. The use of such agents, due to the absence of background signal, could enable a significant improvement in SNR for MR imaging.

In addition to providing a means for signal amplification, nanoparticle imaging agents can further facilitate detection of hard-to-treat cancers by tweaking the biophysical (intravascular transport) and biochemical (receptor targeting) interactions of the nanoparticle with the cancer microenvironment. As we discussed in section 3, the number of ligands on the nanoparticle's surface, the receptor density on the cell's surface, and the nanoparticle's size and shape all impact targeting efficiency [183]. For example, the development of integrin-targeted iron oxide nanochains represent a step towards the rational design of vascular targeted imaging agents [56]. Such an agent has been specifically designed for targeting the microenvironment of micrometastasis. The flexible nanochain particle possesses a unique ability to gain access to and be deposited at micrometastatic sites *via* vascular targeting of the endothelium associated with the disease. The nanochain utilizes ligands to target $\alpha_v\beta_3$ integrin receptors, which are overexpressed on metastatic foci resident in blood vessels [184–190]. The size, shape, and flexibility of the nanochains significantly increase the lateral drift and margination of the particles towards the blood vessel walls in microcirculation (*i.e.*, continuous scavenging of vascular walls) and targeting avidity of nanoparticles (*i.e.*, latching on vascular target) due to geometrically enhanced multivalent attachment on the vascular target. In a mouse model of breast cancer metastasis, a remarkable 6% of the nanochains injected in a mouse model congregated within a micrometastatic site of less than 1 mm in size [92]. In comparison, less than 1% of injected dose of its targeted spherical counterpart reached the micrometastasis. Furthermore, the conjugation of individual iron oxide particles resulted in a construct with higher T2 relaxivity relative to the individual iron oxide nanoparticles. The use of the integrin-targeted nanochain enabled visualization of the early spread of metastatic disease in the liver in a mouse model of metastatic breast cancer (Fig. 7).

Concerns surrounding gadolinium toxicity, specifically in patients with impaired renal function, has also driven investigation into use of altenative nuclei (Mn, Co, Ni) for development of targeted nanoparticle MR agents. Manganese (Mn^{2+} cation), with its five unpaired electrons, has been investigated for development of highly sensitive nanoparticle contrast agents [191, 192]. Stable complexes of manganese oxides (MnO or MN_3O_4) have been synthesized for development of highly efficient Mn-based MRI nanosensors [193]. Multi-function, multimodality upconversion nanoparticles (UCNP) incorporating lanthanides have also been investigated for use in MRI [158, 194–196]. Background-free MRI techniques are gaining considerable interest in the area of novel probe development. Specifically, fluorine-based MRI is gaining increasing attention due to its proximity to the 1H frequency but far enough to perform 'water-less' MRI [197]. 19F nanoparticles have been developed and studied for use in a variety of molecular imaging [198, 199] and cell tracking applications [200, 201]. Silica-based hyperpolarized T1 agents have also been investigated as highly sensitive, background-free contrast agents for use in molecular MRI [202, 203]. The absence of background-signal in both 19F and 29Si MRI enables development of highly sensitive probes/sensors and quantitative imaging techniques, taking MRI into the realm of nuclear imaging.

4.1.4 Targeted Nuclear Imaging Agents—Due to its extraordinary high sensitivity (down to the picomolar level) and quantitative nature, radionuclide-based imaging is considered the standard modality for molecular imaging. Furthermore, there is no tissue penetration limit in comparison to optical imaging. However, a disadvantage of nuclear imaging is that the resolution of either SPECT or PET (~5 mm) is not very high. Even with the inherent high contrast sensitivity of the nuclear imaging techniques, the development of targeted nanoparticles agents has been relatively limited. A popular application of radionuclides has been for monitoring the delivery of nano-therapeutics to solid tumors. For example, image-guided drug delivery systems have been developed by labeling PEGylated liposomal doxorubicin with ^{99m}Tc [204]. ^{111}In-labeled liposomes, conjugated with antibody 2C5, have been used for the *in vivo* gamma imaging of murine Lewis lung carcinoma and 4T1 tumors [205].

Similar to CT, US and MRI, a variety of nanoparticle PET agents for vascular targeting have been investigated. For example, using ^{64}Cu as the radiolabel, mesoporous silica nanoparticles [132] and hollow gold nanospheres [130] have been used for imaging of integrins and CD105, respectively. In terms of SPECT imaging, integrin-targeted gold nanoparticles containing ^{125}I have been developed for SPECT imaging of brain tumors (Fig. 8) [131]. The high contrast sensitivity of this technique enabled rapid tumor signal enhancement i.e., within 10 minutes post-dosing of the targeted agent.

Several other nanoparticle platforms have been investigated for development of targeted nuclear imaging agents. In addition, there has been a growing interest in developing multi-modal contrast agents for use in complementary imaging modalities, such as PET and optical, PET and MRI or SPECT and MRI. In some scenarios, multimodal imaging enables the use of PET for treatment planning with whole-body imaging and the use of optical techniques during therapeutic intervention. For example, a dextran-coated SPIO nanoparticle co-labeled with ^{64}Cu and an NIR fluorophore (Vivotag-680) was used to show the utility of combined Fluorescence Molecular Tomography (FMT) and PET for imaging of tumor associated macrophages (Fig. 9) [206, 207]. Multi-modal RGD-targeted, 64Cu-labeled super-paramagnetic iron oxide (SPIO) nanoparticles have been also reported for PET-MR imaging of drug delivery to solid tumors [208]. Quantum dots (QDs) have been investigated for use as multimodality PET-optical agents. Targeted QDs have been evaluated for imaging of integrins and VEGF receptor over-expressed on tumor blood vessels [209, 210]. Porphyrin platform has also been utilized for development of multi-modal nanoprobes. A ^{64}Cu-porphorysome presented a very stable optical-PET tracer that was able to detect small bone metastases in lower limbs, which were confirmed as malignancies by histology [211]. Targeted mesoporous silica nanoparticles have recently been investigated for PET/optical imaging of tumor angiogenesis [212]. By systemically evaluating the impact of surface engineering, the authors demonstrated a 3-fold increase in tumor targeted as compared to their non-targeted counterparts. Single-walled carbon nanotubes (SWNTs) have been investigated for targeted PET imaging of integrins over-expressed on U87 glioblastoma cells and tumor endothelium [213]. Antibody-labeled 89Zr-SWNT targeting the monomeric vascular endothelial-cadherin (VE-cad) epitope, expressed on tumor angiogenic blood vessels, have also been developed for PET imaging and radiotherapy of tumor vasculature [214]. More recently, targeted upconversion nanoparticles (NaGdF4:Yb3+/Er3+ nanophosphors) presenting RGD peptides have been investigated for pre-clinical multi-modal imaging of tumor angiogenesis in a mouse model of brain tumor using optical, MRI and PET modalities [195]. The study demonstrated good correlation in nanoparticle distribution within tumors as assessed using MRI and PET. T1-based $\alpha_v\beta_3$-targeted ^{99m}Tc-

Gd nanoparticles have been reported for SPECT-MR imaging of tumor angiogenesis. The high contrast sensitivity of SPECT enabled detection of small lesions, while the vascular-targeted MR component facilitated 3D characterization of neovasculature [149]. ^{111}In-perfluorocarbon nanoparticles have also been investigated as a multimodal PET-MR agent [133].

4.1.5 Targeted Optical Agents—Optical imaging is attractive due its high sensitivity, lack of nonionizing radiation, cost-effectiveness and potential for real-time imaging. However, its major disadvantage is the penetration depth of light prohibiting deep tissue imaging in humans. Thus, near-infrared fluorescent (NIRF) imaging has been primarily applied in small-animal imaging, for which several probes have been developed. These probes include synthetic fluorophores, semiconductor fluorescent crystals, and probes based on lanthanide rare-earth ions [215]. Quantum dots have also been investigated in pre-clinical applications; however, their clinical utility has been challenging due to toxicity concerns.

The encapsulation of NIR dyes in nanoparticles has been explored as a method for optical imaging to overcome limitations of free, small-molecule dyes. A number of nanocarriers, including liposomes, silica, and polymersomes have been used for encapsulation of NIR dyes and targeted to a wide range of cancer cells [216]. Furthermore, targeted rare-earth nanocrystals have also been investigated for use as an alternative to heavy-metal quantum dots [142]. As we mentioned before, optical imaging capabilities have been frequently combined with another mode of imaging capability into the same nanoparticle. For example, dendrimers containing Cy5 (an optical probe), gadolinium (a MR probe), and activatable cell-penetrating peptides for targeting matrix metalloproteinases have been developed for use as multimodal optical-MR imaging agents [144]. Furthermore, SPIO nanoparticles labeled with an NIR fluorochrome have been developed for combined FMT-MR imaging of tumor associated macrophages [217].

Quantum dots (QDs) are a growing area of research for medical imaging, yet concerns about toxicity remain a serious challenge for clinical utility. The following criteria has been proposed for successful design and use of QDs for medical imaging and diagnosis: 1) NIR emission, 2) biocompatibility, 3) stability *in vivo*, 4) ultrasmall size, and 5) clearance through the renal system [146]. A QD, which met the above criteria, was developed and investigated. In a comparison of targeted and non-targeted QDs, it was found that the non-targeted agents extravasated into the tumor interstitium. The non-targeted agents were small enough, however, to wash back out into the bloodstream. These results are in good agreement with our discussion on the deep tissue targeting of nanoparticles in section 3.4, which illustrated the poor retention of smaller nanoparticle agents inside the tumor. Targeted QDs, however, resulted in high signal intensity from the tumor site even 24 h after injection [146]. Because of their high signal intensity, targeted QDs also can efficiently image prostate cancer cells and head-and-neck squamous cancer cells [147, 218].

Besides fluorescent imaging, the excellent surface plasmon resonance properties of metallic nanoparticles have been exploited to develop optical imaging agents [219]. Several gold-based nanoparticles have been developed for targeted optical imaging, such as gold nanoparticles and gold nanocages targeting EGFR [134–136, 220, 221], gold nanoshells targeting HER2 [137, 138], and anti-EGFR nanorods [139, 140].

Another new modality related to optical imaging is photoacoustic imaging (PAI), which has the potential for both functional and molecular imaging [143]. While PAI is able to achieve endogenous contrast, based on the differences in absorption spectra of different tissues, exogenous contrast agents are needed for molecular imaging. For generation of contrast, PAI can take advantage of plasmonic nanoparticles (gold nanoshells, nanorods or nanocages) or nonplasmonic nanoparticles with very strong light absorption. Multimodal imaging agents combining PAI with other modalities have also been evaluated [141]. A triple-modality imaging agent has also been developed for imaging brain tumor margins during intervention, using PAI, MRI and Raman spectroscopy [222]. Notably, in an animal model of ovarian cancer, NIRF-labeled SPIO nanoparticles targeted to Her-2/neu receptor enabled acquisition of high-resolution images with a five-fold increase in PA contrast, and significant contrast with FMT imaging. As we will discuss in section 4.3, the combination of PAI and FMT may be advantageous as an intraoperative technique, even for tumors that are located deep within tissue [145].

4.2 Nanotheranostics and image-guided therapies

Historically, nanoparticle-based therapeutics have been labeled with a radioisotope during the initial phases of clinical studies to perform pharmacokinetic and biodistribution studies. In the recent past, however, a new class of nanoparticles has emerged, called nanotheranostics. In addition to the targeted delivery of drugs, these nanoparticles are equipped with imaging functionality, which simultaneously can facilitate treatment and diagnosis, image-guided therapy, or monitoring of the outcome of the therapy. Indeed, at first read, this multifunctionality appears very attractive and hence generates enormous excitement and attention. However, two critical concerns have emerged. In which clinical scenarios does the ability of simultaneous therapy and imaging influence the decision-making process of the oncologist? Second, is the imaging and/or therapeutic performance of a nanoparticle compromise, when the two functions are merged together into the same nanoparticle? Unfortunately, in many instances, these two concerns are somewhat ignored in the preclinical development of nanotheranostic agents.

The initial preclinical demonstration of the utility of nanotheranostics was focused on using imaging to longitudinally monitor the deposition of nanoparticles into tumors and the outcome of cancer treatments. This stems from the fact that tumors exhibit heterogeneities in their microenvironments, which affects the intratumoral delivery of nanoparticles not only from one tumor to the next but also regionally within the same tumor. As a result, these agents can pave the way for more personalized medicine in cancer treatment [223]. Unlike conventional agents, nanoparticle-based imaging agents provide a more accurate assessment of drug dose painting, especially for nano-chemotherapeutics. For example, liposomal CT agents have been used as prognosticating agents for monitoring the effects of PEGylated liposomal doxorubicin (PLD) in breast cancer [29]. Since tumors exhibit significant variability in nanoparticle uptake, the availability of such agents for clinical use could greatly improve the management of cancer patients since it provides a novel method to identify, *a priori*, patients that would respond to nano-chemotherapeutics. In addition, the tumor uptake rate of these particles has also been shown to correlate well with expression levels of angiogenic biomarkers [32]. Similar liposomal CT agents have also been used to assess changes in vascular permeability of tumors due to injury after radiation therapy [224]. Due to their long circulation property and nano-size, these agents provide a more accurate measurement of fractional tumor blood volume and therefore could serve as a phenotypical biomarker to assess the efficacy of anti-angiogenic agents [225].

Similar approaches have also been evaluated using nanoparticles with MR capabilities [226–234]. These studies used various types of nanoparticles, which include ultrasmall superparamagnetic iron oxide (USPIO) particles, iron oxide nanoworms, liposomes and dendrimers. The therapeutic strategies have ranged from chemotherapy (*e.g.* taxanes and anthracyclines) [226, 229, 230] and small interfering RNA [233] to antiangiogenic approaches using the CREKA polypeptide and vascular blockade [232], while the target sites included the folate receptor [227, 229], urokinase plasminogen activator receptor [231], integrins [228, 234], prostate-specific membrane antigen [228]. In addition to MR, theranostic agents have been developed using radioisotopes for SPECT and PET imaging [235–237]. These agents provide attractive features for expedited clinical translation, such as high sensitivity, accurate quantification, and the ability to conduct deep tissue imaging.

However, while the imaging capability of nanotheranostic agents is typically demonstrated by using imaging with MRI, SPECT or PET to indicate the accumulation of an agent in tumors, the benefit of this additional function of the nanoparticle is not always clearly demonstrated in terms of monitoring of the therapeutic outcome or improved image-guided interventions. First, a critical question often remains unanswered: What was the degree of sacrifice of the nanoparticle's therapeutic or imaging capability? A nanotheranostic agent is typically a compromise between the imaging and the therapeutic component of the nanoparticle [238], since significantly different concentrations of the two components are required to perform their corresponding functions. In order to justify the additional complexity in terms of fabrication, cost and regulatory procedures, it is essential to clearly demonstrate the personalized, tumor-specific strategy and the added value and potential clinical benefits of the additional imaging functionality. The value of a nanotheranostic should be determined by metrics which include the extent that patient management is improved, side effects are reduced, and patient outcomes are improved [238].

In addition to drug dose painting, targeted nanotheranostic agents seem to be an ideal fit for photothermal ablation and photodynamic strategies. Following systemic administration of such agents, a subsequent intervention (laser or NIR light) must be applied at the specific target site. Thus, it is critical to be able to detect the exact location of the tumor as well as the presence of the photoabsorber or photosensitizer before application of irradiation. Furthermore, it can be very advantageous to monitor therapeutic progress in real-time to ensure complete eradication of the tumor. Theranostic examples of photothermal therapies using an NIR laser include gold nanoparticles [239, 240] and heparin-folic acid nanoparticles incorporating the IR-780 dye have been demonstrated [241]. Using nanoparticles with MRI capabilities and photodynamic therapy, it has also been demonstrated that MR imaging could reveal the intratumoral location of a silica-based nanoparticle loaded with a photosensitizer [242] or a fullerene nanoparticle (photosensitizer) with its surface functionalized with iron oxide nanoparticles [243]. Imaging also can assist clinicians with the surgical resection of locally invasive tumor lesions, especially in cases where aggressive surgery cannot be performed (*e.g.* brain cancer). It is apparent that identification of the invasive edges of a tumor can significantly improve the outcome of surgeries and reduce the incidence of local recurrence. Typically, such targeted agents are labeled with NIR-dyes to enable intraoperative optical imaging [244]. In this context, we have shown examples of multimodal nanoparticles for PET-optical imaging in section 4.1.4. Such agents can facilitate treatment planning with whole-body imaging and the use of optical techniques during surgery to identify the invasive edges of the tumor.

5. Increasing the Clinical Translation of Targeted Nanotechnologies for Cancer Imaging

The ultimate goal of developing novel imaging agents should be to see their translation to the clinic and subsequently access to patients to enable improvement in health care. The majority of efforts in the development of imaging agents, primarily in the academic domain, have typically been driven by the need to demonstrate scientific novelty. While this will continue to be the primary engine of scientific discovery, the path to clinical translation and regulatory approval for imaging agents requires careful consideration of several factors that go well beyond pre-clinical efficacy studies. Furthermore, the timeline and overall cost of product development for imaging agents is relatively long and expensive, primarily because of the need to acquire a large clinical safety database prior to regulatory approval [245, 246]. Although agents are undergoing development, no nanoparticle imaging agents are currently approved for clinical use. Some of the key factors that need to be considered in the early-stages of imaging agent development are:

- Does the novel agent address an unmet medical need?
- Pre-clinical evaluation of safety and toxicity
- Pre-clinical efficacy evaluation
- Developing a robust chemistry, manufacturing and controls (CMC) program for manufacturing of nanoparticle imaging agent, eventually leading to the production of clinical and commercial-grade material using good manufacturing practices (GMP)
- Identifying the appropriate primary clinical indication

Unlike nano-chemotherapeutics where the target population is cancer patients, depending on the pursued clinical indication for the imaging agent under development, the target population could include healthy subjects. As a result, the threshold for safety margin is higher and therefore an understanding of safety and toxicity in pre-clinical stage as well as during clinical trial is of paramount importance for assessing the benefit-to-risk ratio. The design and conduct of clinical trials for demonstrating the clinical effectiveness of a new imaging agent in terms of substantial improvement in patient management is also becoming an important factor in obtaining regulatory approval [247]. The requirements for demonstrating clinical effectiveness, which goes well beyond the metrics of sensitivity and specificity, becomes even more important for targeted imaging agents since the decision for patient management is driven from the review of images [238]. From a product development perspective, several challenges lie in the development of nanoparticle imaging agent. The majority of approved imaging agents are low molecular weight compounds with a relatively short in vivo residence time. Nanoparticle imaging agents are likely going to demonstrate in vivo pharmacokinetics and distribution that are fundamentally different from the conventional agents these factors need to be considered during the pre-clinical safety evaluation of product development. Nanoparticle agents also pose new safety considerations that need to be considered during product development [248, 249]. One issue that has presented challenges in the development of nanoparticle-based agents is the risk for infusion reactions, sometimes referred to as complement-activation related pseudoallergy (CARPA) [250]. Finally, with the ever-changing landscape surrounding health care, cost-effectiveness of novel imaging agent compared to standard of care and product re-imbursement post-market approval also needs to be taken into consideration during the later stages of product development.

6. Concluding Remarks

Initially, nanoscientists were asking the question what nanotechnology could make. However, in the recent past, the objective has changed to what nanotechnology should be making in order to achieve significant clinical impact. In addition to the significant advantages of contrast sensitivity, multivalency, binding avidity and overall specificity and sensitivity of nanoparticles, appropriate design rules can improve prognosis and facilitate diagnosis with quantitative precision of the most aggressive forms of cancer, which will lead to an overall increase in quality of life and patient outcome.

Even though different nanoparticles exhibit variable *in vivo* behaviors, the process of translation from lab bench to bedside requires further streamlining. Along these lines, it is critical to identify “targets” that have a high likelihood of influencing the decision-making process of clinicians. Therefore, it is essential to avoid poorly designed preclinical studies that lack clear clinical relevance or a well-defined endpoint. Furthermore, another major barrier to translation is the time-consuming and costly animal work required for the necessary safety studies required by FDA. A public database could be established to enable investigators to share data from such studies to avoid redundancy in similar studies.

In conclusion, to realize the full promise of targeted nanotechnology for cancer imaging, it is essential to create an unbiased system to evaluate different nanoparticle imaging agents for the same target and identify the lead nanoparticle. Implementation of such strategy can lead to the development of innovative nanotechnologies for imaging with widespread use in the clinic.

Acknowledgments

This work was supported by grants from the National Cancer Institute (R01CA177716), the Clinical and Translational Science Collaborative of Cleveland (UL1TR000439) from the National Center for Advancing Translational Sciences component of the National Institutes of Health, and the Ohio Cancer Research Associates (E.K.). R.T. was supported by a fellowship from the NIH Interdisciplinary Biomedical Imaging Training Program

(T32EB007509), and L.B. was supported by a fellowship from the National Cancer Institute Training Program in Cancer Pharmacology (R25CA148052).

References

1. Ferrari M. Cancer nanotechnology: opportunities and challenges. Nat Rev Cancer. 2005; 5:161–171. [PubMed: 15738981]
2. Altundag K, Dede DS, Purnak T. Albumin-bound paclitaxel (ABI-007; Abraxane) in the management of basal-like breast carcinoma. J Clin Pathol. 2007; 60:958. [PubMed: 17660346]
3. Chakravarthy AB, Kelley MC, McLaren B, Truica CI, Billheimer D, Mayer IA, Grau AM, Johnson DH, Simpson JF, Beauchamp RD, Jones C, Pietenpol JA. Neoadjuvant Concurrent Paclitaxel and Radiation in Stage II/III Breast Cancer. Clin Cancer Res. 2006; 12:1570–1576. [PubMed: 16533783]
4. Heath JR, Davis ME. Nanotechnology and Cancer. Annu Rev Med. 2007
5. Campos S. Liposomal anthracyclines: adjuvant and neoadjuvant therapy for breast cancer. Oncologist. 2003; 8(Suppl 2):10–16. [PubMed: 13679591]
6. Maeda H, Wu J, Sawa T, Matsumura Y, Hori K. Tumor vascular permeability and the EPR effect in macromolecular therapeutics: a review. J Control Release. 2000; 65:271–284. [PubMed: 10699287]
7. Gradishar WJ, Tjulandin S, Davidson N, Shaw H, Desai N, Bhar P, Hawkins M, O'Shaughnessy J. Phase III trial of nanoparticle albumin-bound paclitaxel compared with polyethylated castor oil-based paclitaxel in women with breast cancer. J Clin Oncol. 2005; 23:7794–7803. [PubMed: 16172456]
8. Lasic DD. Doxorubicin in sterically stabilized liposomes. Nature. 1996; 380:561–562. [PubMed: 8606781]
9. Lasic DD, Papahadjopoulos D. Liposomes revisited. Science. 1995; 267:1275–1276. [PubMed: 7871422]
10. Safra T. Cardiac safety of liposomal anthracyclines. Oncologist. 2003; 8(Suppl 2):17–24. [PubMed: 13679592]
11. Park K. Facing the Truth about Nanotechnology in Drug Delivery. ACS Nano. 2013; 7:7442–7447. [PubMed: 24490875]
12. Schroeder A, Heller DA, Winslow MM, Dahlman JE, Pratt GW, Langer R, Jacks T, Anderson DG. Treating metastatic cancer with nanotechnology. Nat Rev Cancer. 2012; 12:39–50. [PubMed: 22193407]
13. Adiseshaiah PP, Hall JB, McNeil SE. Nanomaterial standards for efficacy and toxicity assessment. Wiley Interdiscip Rev Nanomed Nanobiotechnol. 2010; 2:99–112. [PubMed: 20049834]
14. Kinkel K, Lu Y, Both M, Warren RS, Thoeni RF. Detection of hepatic metastases from cancers of the gastrointestinal tract by using noninvasive imaging methods (US, CT, MR imaging, PET): a meta-analysis. Radiology. 2002; 224:748–756. [PubMed: 12202709]
15. Bipat S, van Leeuwen MS, Comans EF, Pijl ME, Bossuyt PM, Zwinderman AH, Stoker J. Colorectal liver metastases: CT, MR imaging, and PET for diagnosis--meta-analysis. Radiology. 2005; 237:123–131. [PubMed: 16100087]
16. Niekel MC, Bipat S, Stoker J. Diagnostic imaging of colorectal liver metastases with CT, MR imaging, FDG PET, and/or FDG PET/CT: a meta-analysis of prospective studies including patients who have not previously undergone treatment. Radiology. 2011; 257:674–684. [PubMed: 20829538]
17. Cancer facts and figures 2011. American Cancer Society; 2011.
18. Pantel K, Alix-Panabieres C, Riethdorf S. Cancer micrometastases. Nat Rev Clin Oncol. 2009; 6:339–351. [PubMed: 19399023]
19. Robinson PJ. The early detection of liver metastases. Cancer Imaging. 2002; 2:1–3.
20. A.C. Society. Cancer Facts and Figures. 2012.
21. Yuan F, Leunig M, Huang SK, Berk DA, Papahadjopoulos D, Jain RK. Microvascular permeability and interstitial penetration of sterically stabilized (stealth) liposomes in a human tumor xenograft. Cancer Res. 1994; 54:3352–3356. [PubMed: 8012948]

22. Hobbs SK, Monsky WL, Yuan F, Roberts WG, Griffith L, Torchilin VP, Jain RK. Regulation of transport pathways in tumor vessels: role of tumor type and microenvironment. Proc Natl Acad Sci U S A. 1998; 95:4607–4612. [PubMed: 9539785]

23. Jain RK. Transport of molecules, particles, and cells in solid tumors. Annual review of biomedical engineering. 1999; 1:241–263.

24. Fukumura D, Jain RK. Tumor microenvironment abnormalities: causes, consequences, and strategies to normalize. Journal of cellular biochemistry. 2007; 101:937–949. [PubMed: 17171643]

25. McDonald DM, Thurston G, Baluk P. Endothelial gaps as sites for plasma leakage in inflammation. Microcirculation. 1999; 6:7–22. [PubMed: 10100186]

26. McDonald DM, Choyke PL. Imaging of angiogenesis: from microscope to clinic. Nat Med. 2003; 9:713–725. [PubMed: 12778170]

27. Hashizume H, Baluk P, Morikawa S, McLean JW, Thurston G, Roberge S, Jain RK, McDonald DM. Openings between defective endothelial cells explain tumor vessel leakiness. Am J Pathol. 2000; 156:1363–1380. [PubMed: 10751361]

28. McDonald DM, Baluk P. Significance of blood vessel leakiness in cancer. Cancer Res. 2002; 62:5381–5385. [PubMed: 12235011]

29. Karathanasis E, Suryanarayanan S, Balusu SR, McNeeley K, Sechopoulos I, Karellas A, Annapragada AV, Bellamkonda RV. Imaging Nanoprobe for Prediction of Outcome of Nanoparticle Chemotherapy by Using Mammography. Radiology. 2009; 250:398–406. [PubMed: 19188313]

30. Toy R, Hayden E, Camann A, Berman Z, Vicente P, Tran E, Meyers J, Pansky J, Peiris PM, Wu H, Exner A, Wilson D, Ghaghada KB, Karathanasis E. Multimodal in vivo imaging exposes the voyage of nanoparticles in tumor microcirculation. ACS Nano. 2013; 7:3118–3129. [PubMed: 23464827]

31. Yuan F, Chen Y, Dellian M, Safabakhsh N, Ferrara N, Jain RK. Time-dependent vascular regression and permeability changes in established human tumor xenografts induced by an anti-vascular endothelial growth factor/vascular permeability factor antibody. Proc Natl Acad Sci U S A. 1996; 93:14765–14770. [PubMed: 8962129]

32. Karathanasis E, Chan L, Karumbaiah L, McNeeley K, D'Orsi CJ, Annapragada AV, Sechopoulos I, Bellamkonda RV. Tumor vascular permeability to a nanoprobe correlates to tumor-specific expression levels of angiogenic markers. PLoS ONE. 2009; 4:e5843. [PubMed: 19513111]

33. Lee HJ, Cho HY, Oh JH, Namkoong K, Lee JG, Park JM, Lee SS, Huh N, Choi JW. Simultaneous capture and in situ analysis of circulating tumor cells using multiple hybrid nanoparticles. Biosensors & bioelectronics. 47:508–514.

34. Huang YY, Hoshino K, Chen P, Wu CH, Lane N, Huebschman M, Liu H, Sokolov K, Uhr JW, Frenkel EP, Zhang JX. Immunomagnetic nanoscreening of circulating tumor cells with a motion controlled microfluidic system. Biomed Microdevices. 15:673–681. [PubMed: 23109037]

35. Chauhan VP, Jain RK. Strategies for advancing cancer nanomedicine. Nature materials. 2013; 12:958–962.

36. Piner RD, Zhu J, Xu F, Hong S, Mirkin CA. "Dip-Pen" nanolithography. Science. 1999; 283:661–663. [PubMed: 9924019]

37. Canelas DA, Herlihy KP, DeSimone JM. Top-down particle fabrication: control of size and shape for diagnostic imaging and drug delivery. Wiley Interdiscip Rev Nanomed Nanobiotechnol. 2009; 1:391–404. [PubMed: 20049805]

38. Toy R, Peiris PM, Ghaghada KB, Karathanasis E. Shaping cancer nanomedicine: the effect of particle shape on the in vivo journey of nanoparticles. Nanomedicine (Lond). 2014; 9:121–134. [PubMed: 24354814]

39. Toy R, Hayden E, Shoup C, Baskaran H, Karathanasis E. The effects of particle size, density and shape on margination of nanoparticles in microcirculation. Nanotechnology. 2011; 22:115101. [PubMed: 21387846]

40. Thompson AJ, Mastria EM, Eniola-Adefeso O. The margination propensity of ellipsoidal micro/nanoparticles to the endothelium in human blood flow. Biomaterials. 34:5863–5871. [PubMed: 23642534]

41. Namdee K, Thompson AJ, Charoenphol P, Eniola-Adefeso O. Margination propensity of vascular-targeted spheres from blood flow in a microfluidic model of human microvessels. Langmuir. 2013; 29:2530–2535. [PubMed: 23363293]

42. Owens DE 3rd, Peppas NA. Opsonization, biodistribution, and pharmacokinetics of polymeric nanoparticles. International journal of pharmaceutics. 2006; 307:93–102. [PubMed: 16303268]

43. Moghimi SM, Szebeni J. Stealth liposomes and long circulating nanoparticles: critical issues in pharmacokinetics, opsonization and protein-binding properties. Prog Lipid Res. 2003; 42:463–478. [PubMed: 14559067]

44. Litzinger DC, Buiting AM, van Rooijen N, Huang L. Effect of liposome size on the circulation time and intraorgan distribution of amphipathic poly(ethylene glycol)-containing liposomes. Biochim Biophys Acta. 1994; 1190:99–107. [PubMed: 8110825]

45. Nagayasu A, Uchiyama K, Kiwada H. The size of liposomes: a factor which affects their targeting efficiency to tumors and therapeutic activity of liposomal antitumor drugs. Adv Drug Deliv Rev. 1999; 40:75–87. [PubMed: 10837781]

46. Ma X, Wu Y, Jin S, Tian Y, Zhang X, Zhao Y, Yu L, Liang XJ. Gold nanoparticles induce autophagosome accumulation through size-dependent nanoparticle uptake and lysosome impairment. ACS Nano. 5:8629–8639. [PubMed: 21974862]

47. Chithrani BD, Ghazani AA, Chan WC. Determining the size and shape dependence of gold nanoparticle uptake into mammalian cells. Nano Lett. 2006; 6:662–668. [PubMed: 16608261]

48. Kibria G, Hatakeyama H, Ohga N, Hida K, Harashima H. The effect of liposomal size on the targeted delivery of doxorubicin to Integrin alphavbeta3-expressing tumor endothelial cells. Biomaterials. 34:5617–5627. [PubMed: 23623323]

49. Champion JA, Mitragotri S. Role of target geometry in phagocytosis. Proc Natl Acad Sci U S A. 2006; 103:4930–4934. [PubMed: 16549762]

50. Arnida, Janat-Amsbury MM, Ray A, Peterson CM, Ghandehari H. Geometry and surface characteristics of gold nanoparticles influence their biodistribution and uptake by macrophages. Eur J Pharm Biopharm. 77:417–423. [PubMed: 21093587]

51. Huang X, Li L, Liu T, Hao N, Liu H, Chen D, Tang F. The shape effect of mesoporous silica nanoparticles on biodistribution, clearance, and biocompatibility in vivo. ACS Nano. 2011; 5:5390–5399. [PubMed: 21634407]

52. Shapiro, EGaM. Particles in a Shear Flow Near a Solid Wall: Effect of Nonsphericity on Forces and Velocities. Int J Multiphase Flow. 1996

53. Adriani G, de Tullio MD, Ferrari M, Hussain F, Pascazio G, Liu X, Decuzzi P. The preferential targeting of the diseased microvasculature by disk-like particles. Biomaterials. 33:5504–5513. [PubMed: 22579236]

54. Doshi N, Prabhakarpandian B, Rea-Ramsey A, Pant K, Sundaram S, Mitragotri S. Flow and adhesion of drug carriers in blood vessels depend on their shape: a study using model synthetic microvascular networks. J Control Release. 146:196–200. [PubMed: 20385181]

55. Lee SY, Ferrari M, Decuzzi P. Shaping nano-/micro-particles for enhanced vascular interaction in laminar flows. Nanotechnology. 2009; 20:495101, 11. [PubMed: 19904027]

56. Peiris PM, Toy R, Doolittle E, Pansky J, Abramowski A, Tam M, Vicente P, Tran E, Hayden E, Camann A, Mayer A, Erokwu BO, Berman Z, Wilson D, Baskaran H, Flask RA, Keri CA, Karathanasis E. Imaging metastasis using an integrin-targeting chain-shaped nanoparticle. ACS Nano. 2012; 6:8783–8795. [PubMed: 23005348]

57. Shuvaev VV, Ilies MA, Simone E, Zaitsev S, Kim Y, Cai S, Mahmud A, Dziubla T, Muro S, Discher DE, Muzykantov VR. Endothelial targeting of antibody-decorated polymeric filomicelles. ACS Nano. 2011; 5:6991–6999. [PubMed: 21838300]

58. Kolhar P, Anselmo AC, Gupta V, Pant K, Prabhakarpandian B, Ruoslahti E, Mitragotri S. Using shape effects to target antibody-coated nanoparticles to lung and brain endothelium. Proc Natl Acad Sci U S A.

59. Valencia PM, Pridgen EM, Rhee M, Langer R, Farokhzad OC, Karnik R. Microfluidic platform for combinatorial synthesis and optimization of targeted nanoparticles for cancer therapy. ACS Nano. 7:10671–10680. [PubMed: 24215426]

60. Stefanick JF, Ashley JD, Kiziltepe T, Bilgicer B. A systematic analysis of peptide linker length and liposomal polyethylene glycol coating on cellular uptake of peptide-targeted liposomes. ACS Nano. 7:2935–2947. [PubMed: 23421406]

61. Ghaghada KB, Saul J, Natarajan JV, Bellamkonda RV, Annapragada AV. Folate targeting of drug carriers: a mathematical model. J Control Release. 2005; 104:113–128. [PubMed: 15866339]

62. Smith BR, Kempen P, Bouley D, Xu A, Liu Z, Melosh N, Dai H, Sinclair R, Gambhir SS. Shape matters: intravital microscopy reveals surprising geometrical dependence for nanoparticles in tumor models of extravasation. Nano Lett. 2012; 12:3369–3377. [PubMed: 22650417]

63. Smith BR, Cheng Z, De A, Rosenberg J, Gambhir SS. Dynamic visualization of RGD-quantum dot binding to tumor neovasculature and extravasation in multiple living mouse models using intravital microscopy. Small. 2010; 6:2222–2229. [PubMed: 20862677]

64. Smith BR, Cheng Z, De A, Koh AL, Sinclair R, Gambhir SS. Real-time intravital imaging of RGD-quantum dot binding to luminal endothelium in mouse tumor neovasculature. Nano Lett. 2008; 8:2599–2606. [PubMed: 18386933]

65. McNeeley KM, Annapragada A, Bellamkonda RV. Decreased circulation time offsets increased efficacy of PEGylated nanocarriers targeting folate receptors of glioma. Nanotechnology. 2007; 18:385101.

66. Gabizon A, Horowitz AT, Goren D, Tzemach D, Shmeeda H, Zalipsky S. In vivo fate of folate-targeted polyethylene-glycol liposomes in tumor-bearing mice. Clinical Cancer Research. 2003; 9:6551–6559. [PubMed: 14695160]

67. Gabizon A, Shmeeda H, Horowitz AT, Zalipsky S. Tumor cell targeting of liposome-entrapped drugs with phospholipid-anchored folic acid PEG conjugates. Adv Drug Deliv Rev. 2004; 56:1177–1192. [PubMed: 15094214]

68. Pastorino F, Brignole C, Marimpietri D, Cilli M, Gambini C, Ribatti D, Longhi R, Allen TM, Corti A, Ponzoni M. Vascular damage and anti-angiogenic effects of tumor vessel-targeted liposomal chemotherapy. Cancer Res. 2003; 63:7400–7409. [PubMed: 14612539]

69. Maeda H. The enhanced permeability and retention (EPR) effect in tumor vasculature: the key role of tumor-selective macromolecular drug targeting. Advances in enzyme regulation. 2001; 41:189–207. [PubMed: 11384745]

70. Mayer LD, Tai LC, Ko DS, Masin D, Ginsberg RS, Cullis PR, Bally MB. Influence of vesicle size, lipid composition, and drug-to-lipid ratio on the biological activity of liposomal doxorubicin in mice. Cancer Res. 1989; 49:5922–5930. [PubMed: 2790807]

71. Perrault SD, Walkey C, Jennings T, Fischer HC, Chan WC. Mediating tumor targeting efficiency of nanoparticles through design. Nano Lett. 2009; 9:1909–1915. [PubMed: 19344179]

72. Yuan F, Dellian M, Fukumura D, Leunig M, Berk DA, Torchilin VP, Jain RK. Vascular permeability in a human tumor xenograft: molecular size dependence and cutoff size. Cancer Res. 1995; 55:3752–3756. [PubMed: 7641188]

73. Decuzzi P, Causa F, Ferrari M, Netti PA. The effective dispersion of nanovectors within the tumor microvasculature. Ann Biomed Eng. 2006; 34:633–641. [PubMed: 16568349]

74. Decuzzi P, Ferrari M. Design maps for nanoparticles targeting the diseased microvasculature. Biomaterials. 2008; 29:377–384. [PubMed: 17936897]

75. Gentile F, Ferrari M, Decuzzi P. The transport of nanoparticles in blood vessels: the effect of vessel permeability and blood rheology. Ann Biomed Eng. 2008; 36:254–261. [PubMed: 18172768]

76. Netti PA, Roberge S, Boucher Y, Baxter LT, Jain RK. Effect of transvascular fluid exchange on pressure-flow relationship in tumors: a proposed mechanism for tumor blood flow heterogeneity. Microvasc Res. 1996; 52:27–46. [PubMed: 8812751]

77. Nagamitsu A, Greish K, Maeda H. Elevating Blood Pressure as a Strategy to Increase Tumor-targeted Delivery of Macromolecular Drug SMANCS: Cases of Advanced Solid Tumors. Jpn J Clin Oncol. 2009

78. Kong G, Braun RD, Dewhirst MW. Hyperthermia enables tumor-specific nanoparticle delivery: effect of particle size. Cancer Res. 2000; 60:4440–4445. [PubMed: 10969790]

79. Less JR, Skalak TC, Sevick EM, Jain RK. Microvascular network architecture in a mammary carcinoma. Exs. 1992; 61:74–80. [PubMed: 1377578]

80. Jain RK. Determinants of tumor blood flow: a review. Cancer Res. 1988; 48:2641–2658. [PubMed: 3282647]
81. Heldin CH, Rubin K, Pietras K, Ostman A. High interstitial fluid pressure - an obstacle in cancer therapy. Nat Rev Cancer. 2004; 4:806–813. [PubMed: 15510161]
82. Albanese A, Lam AK, Sykes EA, Rocheleau JV, Chan WC. Tumour-on-a-chip provides an optical window into nanoparticle tissue transport. Nat Commun. 4:2718. [PubMed: 24177351]
83. Gavze E, Shapiro M. Motion of inertial spheroidal particles in a shear flow near a solid wall with special application to aerosol transport in microgravity. Journal of Fluid Mechanics. 1998; 371:59–79.
84. Hogg AJ. The inertial migration of non-neutrally buoyant spherical particles in two-dimensional shear flows. Journal of Fluid Mechanics. 1994; 272:285–318.
85. Gentile F, Chiappini C, Fine D, Bhavane RC, Peluccio MS, Cheng MM, Liu X, Ferrari M, Decuzzi P. The effect of shape on the margination dynamics of non-neutrally buoyant particles in two-dimensional shear flows. J Biomech. 2008; 41:2312–2318. [PubMed: 18571181]
86. Gentile F, Curcio A, Indolfi C, Ferrari M, Decuzzi P. The margination propensity of spherical particles for vascular targeting in the microcirculation. J Nanobiotechnology. 2008; 6:9. [PubMed: 18702833]
87. Ghaghada KB, Saul J, Natarajan JV, Bellamkonda RV, Annapragada AV. Folate targeting of drug carriers: A mathematical model. J Control Release. 2005; 104:113–128. [PubMed: 15866339]
88. Psaila B, Lyden D. The metastatic niche: adapting the foreign soil. Nat Rev Cancer. 2009; 9:285–293. [PubMed: 19308068]
89. Wirtz D, Konstantopoulos K, Searson PC. The physics of cancer: the role of physical interactions and mechanical forces in metastasis. Nat Rev Cancer. 2011; 11:512–522. [PubMed: 21701513]
90. Kim YH, Jeon J, Hong SH, Rhim WK, Lee YS, Youn H, Chung JK, Lee MC, Lee DS, Kang KW, Nam JM. Tumor targeting and imaging using cyclic RGD-PEGylated gold nanoparticle probes with directly conjugated iodine-125. Small. 7:2052–2060. [PubMed: 21688390]
91. van Kasteren SI, Campbell SJ, Serres S, Anthony DC, Sibson NR, Davis BG. Glyconanoparticles allow pre-symptomatic in vivo imaging of brain disease. Proc Natl Acad Sci U S A. 2009; 106:18–23. [PubMed: 19106304]
92. Peiris PM, Toy R, Abramowski A, Vicente P, Tucci S, Bauer L, Mayer A, Tam M, Doolittle E, Pansky J, Tran E, Lin D, Schiemann WP, Ghaghada KB, Griswold MA, Karathanasis E. Treatment of cancer micrometastasis using a multicomponent chain-like nanoparticle. J Control Release. 2014; 173:51–58. [PubMed: 24188960]
93. Hainfeld JF, O'Connor MJ, Dilmanian FA, Slatkin DN, Adams DJ, Smilowitz HM. Micro-CT enables microlocalisation and quantification of Her2-targeted gold nanoparticles within tumour regions. Br J Radiol. 2011; 84:526–533. [PubMed: 21081567]
94. Eck W, Nicholson AI, Zentgraf H, Semmler W, Bartling S. Anti-CD4-targeted gold nanoparticles induce specific contrast enhancement of peripheral lymph nodes in X-ray computed tomography of live mice. Nano Lett. 2010; 10:2318–2322. [PubMed: 20496900]
95. Reuveni T, Motiei M, Romman Z, Popovtzer A, Popovtzer R. Targeted gold nanoparticles enable molecular CT imaging of cancer: an in vivo study. Int J Nanomedicine. 2011; 6:2859–2864. [PubMed: 22131831]
96. Chanda N, Kattumuri V, Shukla R, Zambre A, Katti K, Upendran A, Kulkarni RR, Kan P, Fent GM, Casteel SW, Smith CJ, Boote E, Robertson JD, Cutler C, Lever JR, Katti KV, Kannan R. Bombesin functionalized gold nanoparticles show in vitro and in vivo cancer receptor specificity. Proc Natl Acad Sci U S A. 2010; 107:8760–8765. [PubMed: 20410458]
97. Kim D, Jeong YY, Jon S. A Drug-Loaded Aptamer-Gold Nanoparticle Bioconjugate for Combined CT Imaging and Therapy of Prostate Cancer. ACS Nano. 2010; 4:3689–3696. [PubMed: 20550178]
98. Popovtzer R, Agrawal A, Kotov NA, Popovtzer A, Balter J, Carey TE, Kopelman R. Targeted Gold Nanoparticles enable Molecular CT Imaing of Cancer. Nano Lett. 2008; 8:4593–4596. [PubMed: 19367807]

NIH-PA Author Manuscript

NIH-PA Author Manuscript

99. Wang H, Zheng L, Peng C, Guo R, Shen M, Shi X, Zhang G. Computed tomography imaging of cancer cells using acetylated dendrimer-entrapped gold nanoparticles. Biomaterials. 2011; 32:2979–2988. [PubMed: 21277019]

100. Kinsella JM, Jimenez RE, Karmali PP, Rush AM, Kotamraju VR, Gianneschi NC, Ruoslahti E, Stupack D, Sailor MJ. X-ray computed tomography imaging of breast cancer by using targeted peptide-labeled bismuth sulfide nanoparticles. Angew Chem Int Ed Engl. 2011; 50:12308–12311. [PubMed: 22028313]

101. Pan D, Roessl E, Schlomka JP, Caruthers SD, Senpan A, Scott MJ, Allen JS, Zhang H, Hu G, Gaffney PJ, Choi ET, Rasche V, Wickline SA, Proksa R, Lanza GM. Computed tomography in color: NanoK-enhanced spectral CT molecular imaging. Angew Chem Int Ed Engl. 2010; 49:9635–9639. [PubMed: 21077082]

102. Anderson CR, Hu X, Zhang H, Tlaxca J, Decleves A-E, Houghtaling R, Sharma K, Lawrence M, Ferrara KW, Rychak JJ. Ultrasound Molecular Imaging of Tumor Angiogenesis With an Integrin Targeted Microbubble Contrast Agent. Investigative Radiology. 2011; 56:215–224. [PubMed: 21343825]

103. Dayton PA, Pearson D, Clark J, Simon S, Schumann PA, Zutshi R, Matsunaga TO, Ferrara KW. Ultrasonic analysis of peptide- and antibody-targeted microbubble contrast agents for molecular imaging of alphavbeta3-expressing cells. Molecular imaging. 2004; 3:125–134. [PubMed: 15296677]

104. Ellegala DB, Leong-Poi H, Carpenter JE, Klibanov AL, Kaul S, Shaffrey ME, Sklenar J, Lindner JR. Imaging tumor angiogenesis with contrast ultrasound and microbubbles targeted to alpha(v)beta3. Circulation. 2003; 108:336–341. [PubMed: 12835208]

105. Kiessling F, Huppert J, Zhang C, Jayapaul J, Zwick S, Woenne EC, Mueller MM, Zentgraf H, Eisenhut M, Addadi Y, Neeman M, Semmler W. Adhesion and Endocytotic Activity of alpha-v-beta-3-Integrin-expressing Glioma Cells and Only Accumulates in the Vascular Tumor Compartment. Radiology. 2009; 253:462–469. [PubMed: 19789239]

106. Leong-Poi H. Noninvasive Assessment of Angiogenesis by Ultrasound and Microbubbles Targeted to alphav-Integrins. Circulation. 2002; 107:455–460. [PubMed: 12551871]

107. Willmann JK, Kimura RH, Deshpande N, Lutz AM, Cochran JR, Gambhir SS. Targeted contrast-enhanced ultrasound imaging of tumor angiogenesis with contrast microbubbles conjugated to integrin-binding knottin peptides. J Nucl Med. 2010; 51:433–440. [PubMed: 20150258]

108. Pysz MA, Foygel K, Rosenberg J, Gambhir SS, Schneider M, Willmann JK. Antiangiogenic Cancer Therapy: Monitoring with Molecular US and a Clinically Translatable Contrast Agent (BR55). Radiology. 2010; 256:519–527. [PubMed: 20515975]

109. Willmann JK, Lutz AM, Paulmurugan R, Patel MR, Chu P, Rosenberg J, Gambhir SS. Dual-targeted Contrast Agent for US Assessment of Tumor Angiogenesis in Vivo. Radiology. 2008; 248:936–944. [PubMed: 18710985]

110. Zhang C, Jugold M, Woenne EC, Lammers T, Morgenstern B, Mueller MM, Zentgraf H, Bock M, Eisenhut M, Semmler W, Kiessling F. Specific targeting of tumor angiogenesis by RGD-conjugated ultrasmall superparamagnetic iron oxide particles using a clinical 1.5-T magnetic resonance scanner. Cancer research. 2007; 67:1555–1562. [PubMed: 17308094]

111. Lee GY, Qian WP, Wang L, Wang YA, Staley CA, Satpathy M, Nie S, Mao H, Yang L. Theranostic Nanoparticles with Controlled Release of Gemcitabine for Targeted Therapy and MRI of Pancreatic Cancer. ACS Nano. 2013; 7:2078–2089. [PubMed: 23402593]

112. Park J, Kim S, Saw PE, Lee IH, Yu MK, Kim M, Lee K, Kim YC, Jeong YY, Jon S. Fibronectin extra domain B-specific aptide conjugated nanoparticles for targeted cancer imaging. J Control Release. 2012; 163:111–118. [PubMed: 22964395]

113. He Y, Song W, Lei J, Li Z, Cao J, Huang S, Meng J, Xu H, Jin Z, Xue H. Anti-CXCR4 monoclonal antibody conjugated to ultrasmall superparamagnetic iron oxide nanoparticles in an application of MR molecular imaging of pancreatic cancer cell lines. Acta radiologica. 2012; 53:1049–1058. [PubMed: 23012484]

114. Hsieh WJ, Liang CJ, Chieh JJ, Wang SH, Lai IR, Chen JH, Chang FH, Tseng WK, Yang SY, Wu CC, Chen YL. In vivo tumor targeting and imaging with anti-vascular endothelial growth factor antibody-conjugated dextran-coated iron oxide nanoparticles. Int J Nanomedicine. 2012; 7:2833–2842. [PubMed: 22745546]

115. Kresse M, Wagner S, Pfefferer D, Lawaczeck R, Elste V, Semmler W. Targeting of Ultrasmall Superparamagnetic Iron Oxide (USPIO) Particles to Tumor Cells In Vivo by Using Transferrin Receptor Pathways. Magn Reson Med. 1998; 40:236–242. [PubMed: 9702705]

116. John R, Nguyen FT, Kolbeck KJ, Chaney EJ, Marjanovic M, Suslick KS, Boppart SA. Targeted multifunctional multimodal protein-shell microspheres as cancer imaging contrast agents. Mol Imaging Biol. 2012; 14:17–24. [PubMed: 21298354]

117. Mulder WJ, Strijkers GJ, Habets JW, Bleeker EJ, van der Schaft DW, Storm G, Koning GA, Griffioen AW, Nicolay K. MR molecular imaging and fluorescence microscopy for identification of activated tumor endothelium using a bimodal lipidic nanoparticle. FASEB J. 2005; 19:2008–2010. [PubMed: 16204353]

118. Mulder WJ, van der Schaft DW, Hautvast PA, Strijkers GJ, Koning GA, Storm G, Mayo KH, Griffioen AW, Nicolay K. Early in vivo assessment of angiostatic therapy efficacy by molecular MRI. FASEB journal : official publication of the Federation of American Societies for Experimental Biology. 2007; 21:378–383. [PubMed: 17202248]

119. Kluza E, Jacobs I, Hectors SJ, Mayo KH, Griffioen AW, Strijkers GJ, Nicolay K. Dual-targeting of alphavbeta3 and galectin-1 improves the specificity of paramagnetic/fluorescent liposomes to tumor endothelium in vivo. J Control Release. 2012; 158:207–214. [PubMed: 22079810]

120. Kluza E, van der Schaft DW, Hautvast PA, Mulder WJ, Mayo KH, Griffioen AW, Strijkers GJ, Nicolay K. Synergistic targeting of alphavbeta3 integrin and galectin-1 with heteromultivalent paramagnetic liposomes for combined MR imaging and treatment of angiogenesis. Nano Lett. 2010; 10:52–58. [PubMed: 19968235]

121. Paulis LEM, Jacobs I, van den Akker NM, Geelen T, Molin DG, Starmans LWE, Nicolay K, Strijkers GJ. Targeting of ICAM-1 on vascular endothelium under static and shear stress conditions using a liposomal Gd-based MRI contrast agent. J Nanobiotechnology. 2012; 10

122. Zhang D, Feng XY, Henning TD, Wen L, Lu WY, Pan H, Wu X, Zou LG. MR imaging of tumor angiogenesis using sterically stabilized Gd-DTPA liposomes targeted to CD105. European journal of radiology. 2009; 70:180–189. [PubMed: 18541399]

123. Kamaly N, Kalber T, Thanou M, Bell JD, Miller AD. Folate Receptor Targeted Bimodal Liposomes for Tumor Magnetic Resonance Imaging. Bioconjugate Chem. 2009; 20:648–655.

124. Kaneda MM, Caruthers S, Lanza GM, Wickline SA. Perfluorocarbon nanoemulsions for quantitative molecular imaging and targeted therapeutics. Ann Biomed Eng. 2009; 37:1922–1933. [PubMed: 19184435]

125. Schmieder AH, Caruthers SD, Zhang H, Williams TA, Robertson JD, Wickline SA, Lanza GM. Three-dimensional MR mapping of angiogenesis with alpha5beta1(alpha nu beta3)-targeted theranostic nanoparticles in the MDA-MB-435 xenograft mouse model. FASEB journal : official publication of the Federation of American Societies for Experimental Biology. 2008; 22:4179–4189. [PubMed: 18697838]

126. Boles KS, Schmieder AH, Koch AW, Carano RA, Wu Y, Caruthers SD, Tong RK, Stawicki S, Hu G, Scott MJ, Zhang H, Reynolds BA, Wickline SA, Lanza GM. MR angiogenesis imaging with Robo4- vs. alphaVbeta3-targeted nanoparticles in a B16/F10 mouse melanoma model. FASEB journal : official publication of the Federation of American Societies for Experimental Biology. 2010; 24:4262–4270. [PubMed: 20585027]

127. Flament J, Geffroy F, Medina C, Robic C, Mayer JF, Meriaux S, Valette J, Robert P, Port M, Le Bihan D, Lethimonnier F, Boumezbeur F. In vivo CEST MR imaging of U87 mice brain tumor angiogenesis using targeted LipoCEST contrast agent at 7 T. Magn Reson Med. 2013; 69:179–187. [PubMed: 22378016]

128. Konda SD, Aref M, Wang S, Brechbiel M, Wiener EC. Specific targeting of folate-dendrimer MRI contrast agents to the high affinity folate receptor expressed in ovarian tumor xenografts. MAGMA. 2001; 12:104–113. [PubMed: 11390265]

129. Swanson SD, Kukowska-Latalla JF, Patri AK, Chen C, Ge S, Cao Z, Kotlyar A, East AT, Baker JR. Targeted gadolinium-loaded dendrimer nanoparticles for tumor-specific magnetic resonance contrast enhancement. Int J Nanomedicine. 2008; 3:201–210. [PubMed: 18686779]

130. Tian M, Lu W, Zhang R, Xiong C, Ensor J, Nazario J, Jackson J, Shaw C, Dixon KA, Miller J, Wright K, Li C, Gupta S. Tumor uptake of hollow gold nanospheres after intravenous and intra-

arterial injection: PET/CT study in a rabbit VX2 liver cancer model. Mol Imaging Biol. 2013; 15:614–624. [PubMed: 23608932]

131. Kim YH, Jeon J, Hong SH, Rhim WK, Lee YS, Youn H, Chung JK, Lee MC, Lee DS, Kang KW, Nam JM. Tumor targeting and imaging using cyclic RGD-PEGylated gold nanoparticle probes with directly conjugated iodine-125. Small. 2011; 7:2052–2060. [PubMed: 21688390]
132. Chen F, Hong H, Zhang Y, Valdovinos HF, Shi S, Kwon GS, Theuer CP, Barnhart TE, Cai W. In Vivo Tumor Targeting and Image-Guided Drug Delivery with Antibody-Conjugated, Radiolabeled Mesoporous Silica Nanoparticles. ACS Nano. 2013; 7:9027–9039. [PubMed: 24083623]
133. Hu G, Lijowski M, Zhang H, Partlow KC, Caruthers SD, Kiefer G, Gulyas G, Athey P, Scott MJ, Wickline SA, Lanza GM. Imaging of Vx-2 rabbit tumors with alpha(nu)beta3-integrin-targeted 111In nanoparticles. Int J Cancer. 2007; 120:1951–1957. [PubMed: 17278104]
134. Aaron J, Nitin N, Travis K, Kumar S, Collier T, Park SY, Jose-Yacaman M, Coghlan L, Follen M, Richards-Kortum R, Sokolov K. Plasmon resonance coupling of metal nanoparticles for molecular imaging of carcinogenesis in vivo. Journal of biomedical optics. 2007; 12:03400.
135. El-Sayed IH, Huang X, El-Sayed MA. Surface Plasmon Resonance Scattering and Absorption of anti-EGFR Antibody Conjugated Gold Nanoparticles in Cancer Diagnostics: Applications in Oral Cancer. Nano Lett. 2005; 5:829–834. [PubMed: 15884879]
136. Skala MC, Crow MJ, Wax A, Izatt JA. Photothermal Optical Coherence Tomography of Epiderma Growth Factor Receptor in Live Cells Using Immunotargeted Gold Nanospheres. Nano Lett. 2008; 8:3461–3467. [PubMed: 18767886]
137. Loo C, Hirsch L, Lee M-H, Chang E, West J, Halas N, Drezek R. Gold nanoshell bioconjugates for molecular imaging in living cells. Opt Lett. 2005; 30:1012–1014. [PubMed: 15906987]
138. Loo C, Lowery A, Halas N, West J, Drezek R. Immunotargeted Nanoshells for Integrated Cancer Imaging and Therapy. Nano Lett. 2005; 5:709–711. [PubMed: 15826113]
139. Durr NJ, Larson T, Smith DK, Korgel BA, Sokolov K, Ben-Yakar A. Two-Photon Luminescence Imaging of Cancer Cells Using Molecularly Targeted Gold Nanorods. Nano Lett. 2007; 7:941–945. [PubMed: 17335272]
140. Huang X, El-Sayed IH, Qian W, El-Sayed MA. Cancer Cell Imaging and Photothermal Therapy in the Near-Infrared Region by Using Gold Nanorods. Journal of the American Chemical Society. 2006; 128:2115–2120. [PubMed: 16464114]
141. Jokerst JV, Miao Z, Zavaleta C, Cheng Z, Gambhir SS. Affibody-functionalized gold-silica nanoparticles for Raman molecular imaging of the epidermal growth factor receptor. Small. 2011; 7:625–633. [PubMed: 21302357]
142. Setua S, Menon D, Asok A, Nair S, Koyakutty M. Folate receptor targeted, rare-earth oxide nanocrystals for bi-modal fluorescence and magnetic imaging of cancer cells. Biomaterials. 2010; 31:714–729. [PubMed: 19822364]
143. Kim G, Huang SW, Day KC, O'Donnell M, Agayan RR, Day MA, Kopelman R, Ashkenazi S. Indocyanine-green-embedded PEBBLEs as a contrast agent for photoacoustic imaging. Journal of biomedical optics. 2007; 12:04402.
144. Olson ES, Jiang T, Aguilera TA, Nguyen QT, Ellies LG, Scadeng M, Tsien RY. Activatable cell penetrating peptides linked to nanoparticles as dual probes for in vivo fluorescence and MR imaging of proteases. Proc Natl Acad Sci U S A. 2010; 107:4311–4316. [PubMed: 20160077]
145. Xi L, Satpathy M, Zhao Q, Qian W, Yang L, Jiang H. HER-2/neu targeted delivery of a nanoprobe enables dual photoacoustic and fluorescence tomography of ovarian cancer. Nanomedicine : nanotechnology, biology, and medicine. 2013
146. Gao J, Chen K, Luong R, Bouley DM, Mao H, Qiao T, Gambhir SS, Cheng Z. A novel clinically translatable fluorescent nanoparticle for targeted molecular imaging of tumors in living subjects. Nano Lett. 2012; 12:281–286. [PubMed: 22172022]
147. Gao X, Cui Y, Levenson RM, Chung LW, Nie S. In vivo cancer targeting and imaging with semiconductor quantum dots. Nat Biotechnol. 2004; 22:969–976. [PubMed: 15258594]
148. Chen J, Cheng D, Li J, Wang Y, Guo JX, Chen ZP, Cai BC, Yang T. Influence of lipid composition on the phase transition temperature of liposomes composed of both DPPC and HSPC. Drug development and industrial pharmacy. 2013; 39:197–204. [PubMed: 22443684]

149. Lijowski M, Caruthers S, Hu G, Zhang H, Scott MJ, Williams T, Erpelding T, Schmieder AH, Kiefer G, Gulyas G, Athey PS, Gaffney PJ, Wickline SA, Lanza GM. High sensitivity: high-resolution SPECT-CT/MR molecular imaging of angiogenesis in the Vx2 model. Invest Radiol. 2009; 44:15–22. [PubMed: 18836386]

150. Thakor AS, Gambhir SS. Nanooncology: the future of cancer diagnosis and therapy. CA Cancer J Clin. 2013; 63:395–418. [PubMed: 24114523]

151. Penet MF, Artemov D, Farahani K, Bhujwalla ZM. MR - eyes for cancer: looking within an impenetrable disease. NMR Biomed. 2013; 26:745–755. [PubMed: 23784955]

152. Ma D, Gulani V, Seiberlich N, Liu K, Sunshine JL, Duerk JL, Griswold MA. Magnetic resonance fingerprinting. Nature. 2013; 495:187–192. [PubMed: 23486058]

153. Runge VM. Current technological advances in magnetic resonance with critical impact for clinical diagnosis and therapy. Invest Radiol. 2013; 48:869–877. [PubMed: 24126386]

154. Ghaghada KB, Bockhorst KH, Mukundan S Jr, Annapragada AV, Narayana PA. High-resolution vascular imaging of the rat spine using liposomal blood pool MR agent. AJNR Am J Neuroradiol. 2007; 28:48–53. [PubMed: 17213423]

155. Mieszawska AJ, Mulder WJ, Fayad ZA, Cormode DP. Multifunctional gold nanoparticles for diagnosis and therapy of disease. Mol Pharm. 2013; 10:831–847. [PubMed: 23360440]

156. Cormode DP, Naha PC, Fayad ZA. Nanoparticle contrast agents for computed tomography: a focus on micelles. Contrast Media Mol Imaging. 2014; 9:37–52. [PubMed: 24470293]

157. Gu Z, Yan L, Tian G, Li S, Chai Z, Zhao Y. Recent advances in design and fabrication of upconversion nanoparticles and their safe theranostic applications. Adv Mater. 2013; 25:3758–3779. [PubMed: 23813588]

158. Zeng S, Tsang MK, Chan CF, Wong KL, Hao J. PEG modified BaGdF(5):Yb/Er nanoprobes for multi-modal upconversion fluorescent in vivo X-ray computed tomography and biomagnetic imaging. Biomaterials. 2012; 33:9232–9238. [PubMed: 23036962]

159. Ma J, Huang P, He M, Pan L, Zhou Z, Feng L, Gao G, Cui D. Folic acid-conjugated LaF3:Yb,Tm@SiO2 nanoprobes for targeting dual-modality imaging of upconversion luminescence and X-ray computed tomography. J Phys Chem B. 2012; 116:14062–14070. [PubMed: 23134318]

160. Wang C, Cheng L, Liu Z. Upconversion nanoparticles for photodynamic therapy and other cancer therapeutics. Theranostics. 2013; 3:317–330. [PubMed: 23650479]

161. Chien YH, Chou YL, Wang SW, Hung ST, Liau MC, Chao YJ, Su CH, Yeh CS. Near-infrared light photocontrolled targeting, bioimaging and chemotherapy with caged upconversion nanoparticles in vitro and in vivo. ACS Nano. 2013; 7:8516–8528. [PubMed: 24070408]

162. Cui S, Yin D, Chen Y, Di Y, Chen H, Ma Y, Achilefu S, Gu Y. In vivo targeted deep-tissue photodynamic therapy based on near-infrared light triggered upconversion nanoconstruct. ACS Nano. 2013; 7:676–688. [PubMed: 23252747]

163. Pan D, Schirra CO, Senpan A, Schmieder AH, Stacy AJ, Roessl E, Thran A, Wickline SA, Proska R, Lanza GM. An Early Investigation of Ytterbium Nanocolloids for Selective and Quantitative “Multicolor” Spectral CT Imaing. ACS Nano. 2012; 6:3364–3370. [PubMed: 22385324]

164. Oh MH, Lee N, Kim H, Park SP, Piao Y, Lee J, Jun SW, Moon WK, Choi SH, Hyeon T. Large-scale synthesis of bioinert tantalum oxide nanoparticles for X-ray computed tomography imaging and bimodal image-guided sentinel lymph node mapping. J Am Chem Soc. 2011; 133:5508–5515. [PubMed: 21428437]

165. Liu R, Tian B, Gearing M, Hunter S, Ye K, Mao Z. Cdk5-mediated regulation of the PIKE-A-Akt pathway and glioblastoma cell invasion. Proc Natl Acad Sci U S A. 2008; 105:7570–7575. [PubMed: 18487454]

166. Zhou J, Patel TR, Sirianni RW, Strohbehn G, Zheng MQ, Duong N, Schafbauer T, Huttner AJ, Huang Y, Carson RE, Zhang Y, Sullivan DJ Jr, Piepmeier JM, Saltzman WM. Highly penetrative, drug-loaded nanocarriers improve treatment of glioblastoma. Proc Natl Acad Sci U S A. 2013; 110:11751–11756. [PubMed: 23818631]

167. Anderson CR, Rychak JJ, Backer M, Backer J, Ley K, Klibanov AL. scVEGF Microbubble Ultrasound Contrast Agents: A Novel Probe for Ultrasound Molecular Imaging of Tumor Angiogenesis. Investigative Radiology. 2010; 45:579–585. [PubMed: 20733505]

168. Saul JM, Annapragada AV, Bellamkonda RV. A dual-ligand approach for enhancing targeting selectivity of therapeutic nanocarriers. J Control Release. 2006; 114:277–287. [PubMed: 16904220]

169. Bulte JW, Kraitchman DL. Iron oxide MR contrast agents for molecular and cellular imaging. NMR Biomed. 2004; 17:484–499. [PubMed: 15526347]

170. Jun Y-W, Seo J-W, Cheon J. Nanoscaling Laws of Magnetic Nanoparticles and Their Applicabilities in Biomedical Sciences. Accounts of Chemical Research. 2008; 41:179–189. [PubMed: 18281944]

171. Smolensky ED, Park HY, Zhou Y, Rolla GA, Marjanska M, Botta M, Pierre VC. Scaling Laws at the Nano Size: The Effect of Particle Size and Shape on the Magnetism and Relaxivity of Iron Oxide Nanoparticle Contrast Agents. Journal of materials chemistry. B, Materials for biology and medicine. 2013; 1:2818–2828.

172. Artemov D, Mori N, Okollie B, Bhujwalla ZM. MR molecular imaging of the Her-2/neu receptor in breast cancer cells using targeted iron oxide nanoparticles. Magn Reson Med. 2003; 49:403–408. [PubMed: 12594741]

173. Langereis S, Geelen T, Grull H, Strijkers GJ, Nicolay K. Paramagnetic liposomes for molecular MRI and MRI-guided drug delivery. NMR Biomed. 2013; 26:728–744. [PubMed: 23703874]

174. Kelly KA, Allport JR, Tsourkas A, Shinde-Patil VR, Josephson L, Weissleder R. Detection of vascular adhesion molecule-1 expression using a novel multimodal nanoparticle. Circ Res. 2005; 96:327–336. [PubMed: 15653572]

175. Ghaghada KB, Ravoori M, Sabapathy D, Bankson J, Kundra V, Annapragada A. New dual mode gadolinium nanoparticle contrast agent for magnetic resonance imaging. PLoS One. 2009; 4:e7628. [PubMed: 19893616]

176. Kok MB, Strijkers GJ, Nicolay K. Dynamic changes in 1H-MR relaxometric properties of cell-internalized paramagnetic liposomes, as studied over a five-day period. Contrast Media Mol Imaging. 2011; 6:69–76. [PubMed: 20936712]

177. Laurent S, Vander Elst L, Thirifays C, Muller RN. Paramagnetic Liposomes: Inner versus Outer Membrane Relaxivity of DPPC Liposomes Incorporating Lipophilic Gadolinium Complexes. Langmuir. 2008; 24:4347–4351. [PubMed: 18338913]

178. Laurent S, Vander Elst L, Thirifays C, Muller RN. Relaxivities of paramagnetic liposomes: on the importance of the chain type and the length of the amphiphilic complex. European biophysics journal : EBJ. 2008; 37:1007–1014. [PubMed: 18427798]

179. Santra S, Jativa SD, Kaittanis C, Normand G, Grimm J, Perez JM. Gadolinium-Encapsulating Iron Oxide Nanoprobe as Activatable NMR/MRI Contrast Agent. ACS Nano. 2012; 6:7281–7294. [PubMed: 22809405]

180. Opina AC, Ghaghada KB, Zhao P, Kiefer G, Annapragada A, Sherry AD. TmDOTA-tetraglycinate encapsulated liposomes as pH-sensitive LipoCEST agents. PLoS One. 2011; 6:e2737.

181. Castelli DD, Terreno E, Longo D, Aime S. Nanoparticle-based chemical exchange saturation transfer (CEST) agents. NMR Biomed. 2013; 26:839–849. [PubMed: 23784956]

182. Vinogradov E, Sherry AD, Lenkinski RE. CEST: from basic principles to applications, challenges and opportunities. Journal of magnetic resonance. 2013; 229:155–172. [PubMed: 23273841]

183. Elias DR, Poloukhtine A, Popik V, Tsourkas A. Effect of ligand density, receptor density, and nanoparticle size on cell targeting. Nanomedicine : nanotechnology, biology and medicine. 2013; 9:194–201.

184. Gay LJ, Felding-Habermann B. Contribution of platelets to tumour metastasis. Nat Rev Cancer. 2011; 11:123–134. [PubMed: 21258396]

185. Felding-Habermann B, Habermann R, Saldivar E, Ruggeri ZM. Role of beta3 integrins in melanoma cell adhesion to activated platelets under flow. J Biol Chem. 1996; 271:5892–5900. [PubMed: 8621462]

186. McCarty OJ, Mousa SA, Bray PF, Konstantopoulos K. Immobilized platelets support human colon carcinoma cell tethering, rolling, and firm adhesion under dynamic flow conditions. Blood. 2000; 96:1789–1797. [PubMed: 10961878]

187. Arnaout MA, Mahalingam B, Xiong JP. Integrin structure, allostery and bidirectional signaling. Annu Rev Cell Dev Biol. 2005; 21:381–410. [PubMed: 16212500]

188. Felding-Habermann B, O'Toole TE, Smith JW, Fransvea E, Ruggeri ZM, Ginsberg MH, Hughes PE, Pampori N, Shattil SJ, Saven A, Mueller BM. Integrin activation controls metastasis in human breast cancer. Proc Natl Acad Sci U S A. 2001; 98:1853–1858. [PubMed: 11172040]

189. Lorger M, Krueger JS, O'Neal M, Staflin K, Felding-Habermann B. Activation of tumor cell integrin alphavbeta3 controls angiogenesis and metastatic growth in the brain. Proc Natl Acad Sci U S A. 2009; 106:10666–10671. [PubMed: 19541645]

190. Desgrosellier JS, Cheresh DA. Integrins in cancer: biological implications and therapeutic opportunities. Nat Rev Cancer. 2010; 10:9–22. [PubMed: 20029421]

191. Lee JH, Huh YM, Jun YW, Seo JW, Jang JT, Song HT, Kim S, Cho EJ, Yoon HG, Suh JS, Cheon J. Artificially engineered magnetic nanoparticles for ultra-sensitive molecular imaging. Nat Med. 2007; 13:95–99. [PubMed: 17187073]

192. Pan D, Schmieder AH, Wickline SA, Lanza GM. Manganese-based MRI contrast agents: past present and future. Tetrahedron. 2011; 67:8431–8444. [PubMed: 22043109]

193. Baek MJ, Park JY, Xu W, Kattel K, Kim HG, Lee EJ, Patel AK, Lee JJ, Chang Y, Kim TJ, Bae JE, Chae KS, Lee GH. Water-soluble MnO nanocolloid for a molecular T1 MR imaging: a facile one-pot synthesis, in vivo T1 MR images, and account for relaxivities. ACS applied materials & interfaces. 2010; 2:2949–2955. [PubMed: 20929249]

194. Xia A, Chen M, Gao Y, Wu D, Feng W, Li F. Gd3+ complex-modified NaLuF4-based upconversion nanophosphors for trimodality imaging of NIR-to-NIR upconversion luminescence, X-Ray computed tomography and magnetic resonance. Biomaterials. 2012; 33:5394–5405. [PubMed: 22560666]

195. Lee J, Lee TS, Ryu J, Hong S, Kang M, Im K, Kang JH, Lim SM, Park S, Song R. RGD peptide-conjugated multimodal NaGdF4:Yb3+/Er3+ nanophosphors for upconversion luminescence, MR and PET imaging of tumor angiogenesis. J Nucl Med. 2013; 54:96–103. [PubMed: 23232276]

196. Shen JW, Yang CX, Dong LX, Sun HR, Gao K, Yan XP. Incorporation of computed tomography and magnetic resonance imaging function into NaYF4:Yb/Tm upconversion nanoparticles for in vivo trimodal bioimaging. Anal Chem. 2013; 85:12166–12172. [PubMed: 24237132]

197. Chen J, Lanza GM, Wickline SA. Quantitative magnetic resonance fluorine imaging: today and tomorrow. Wiley Interdiscip Rev Nanomed Nanobiotechnol. 2010; 2:431–440. [PubMed: 20564465]

198. Southworth R, Kaneda M, Chen J, Zhang L, Zhang H, Yang X, Razavi R, Lanza G, Wickline SA. Renal vascular inflammation induced by Western diet in ApoE-null mice quantified by (19)F NMR of VCAM-1 targeted nanobeacons. Nanomedicine : nanotechnology, biology, and medicine. 2009; 5:359–367.

199. Giraudeau C, Geffroy F, Meriaux S, Boumezbeur F, Robert P, Port M, Robic C, Le Bihan D, Lethimonnier F, Valette J. 19F molecular MR imaging for detection of brain tumor angiogenesis: in vivo validation using targeted PFOB nanoparticles. Angiogenesis. 2013; 16:171–179. [PubMed: 23053783]

200. Srinivas M, Boehm-Sturm P, Figdor CG, de Vries IJ, Hoehn M. Labeling cells for in vivo tracking using (19)F MRI. Biomaterials. 2012; 33:8830–8840. [PubMed: 22959182]

201. Ahrens ET, Bulte JW. Tracking immune cells in vivo using magnetic resonance imaging. Nature reviews. Immunology. 2013; 13:755–763.

202. Atkins TM, Cassidy MC, Lee M, Ganguly S, Marcus CM, Kauzlarich SM. Synthesis of long T(1) silicon nanoparticles for hyperpolarized (2)(9)Si magnetic resonance imaging. ACS Nano. 2013; 7:1609–1617. [PubMed: 23350651]

203. Cassidy MC, Chan HR, Ross BD, Bhattacharya PK, Marcus CM. In vivo magnetic resonance imaging of hyperpolarized silicon particles. Nat Nanotechnol. 2013; 8:363–368. [PubMed: 23644571]

204. Bao A, Goins B, Klipper R, Negrete G, Phillips WT. Direct 99mTc labeling of pegylated liposomal doxorubicin (Doxil) for pharmacokinetic and non-invasive imaging studies. J Pharmacol Exp Ther. 2004; 308:419–425. [PubMed: 14610219]

205. Elbayoumi TA, Torchilin VP. Enhanced accumulation of long-circulating liposomes modified with the nucleosome-specific monoclonal antibody 2C5 in various tumours in mice: gamma-imaging studies. Eur J Nucl Med Mol Imaging. 2006; 33:1196–1205. [PubMed: 16763815]

206. Nahrendorf M, Zhang H, Hembrador S, Panizzi P, Sosnovik DE, Aikawa E, Libby P, Swirski FK, Weissleder R. Nanoparticle PET-CT imaging of macrophages in inflammatory atherosclerosis. Circulation. 2008; 117:379–387. [PubMed: 18158358]

207. Nahrendorf M, Keliher E, Marinelli B, Waterman P, Feruglio PF, Fexon L, Pivovarov M, Swirski FK, Pittet MJ, Vinegoni C, Weissleder R. Hybrid PET-optical imaging using targeted probes. Proc Natl Acad Sci U S A. 2010; 107:7910–7915. [PubMed: 20385821]

208. Yang X, Hong H, Grailer JJ, Rowland IJ, Javadi A, Hurley SA, Xiao Y, Yang Y, Zhang Y, Nickles RJ, Cai W, Steeber DA, Gong S. cRGD-functionalized, DOX-conjugated, and (6)(4)Cu-labeled superparamagnetic iron oxide nanoparticles for targeted anticancer drug delivery and PET/MR imaging. Biomaterials. 32:4151–4160. [PubMed: 21367450]

209. Cai W, Chen K, Li ZB, Gambhir SS, Chen X. Dual-function probe for PET and near-infrared fluorescence imaging of tumor vasculature. J Nucl Med. 2007; 48:1862–1870. [PubMed: 17942800]

210. Chen K, Li ZB, Wang H, Cai W, Chen X. Dual-modality optical and positron emission tomography imaging of vascular endothelial growth factor receptor on tumor vasculature using quantum dots. Eur J Nucl Med Mol Imaging. 2008; 35:2235–2244. [PubMed: 18566815]

211. Liu TW, MacDonald TD, Jin CS, Gold JM, Bristow RG, Wilson BC, Zheng G. Inherently Multimodal Nanoparticle-Driven Tracking and Real-Time Delineation of Orthotopic Prostate Tumors and Micrometastases. ACS Nano. 2013; 7

212. Chen F, Hong H, Shi S, Goel S, Valdovinos HF, Hernandez R, Theuer CP, Barnhart TE, Cai W. Engineering of hollow mesoporous silica nanoparticles for remarkably enhanced tumor active targeting efficacy. Scientific reports. 2014; 4:5080. [PubMed: 24875656]

213. Liu Z, Cai W, He L, Nakayama N, Chen K, Sun X, Chen X, Dai H. In vivo biodistribution and highly efficient tumour targeting of carbon nanotubes in mice. Nat Nanotechnol. 2007; 2:47–52. [PubMed: 18654207]

214. Ruggiero A, Villa CH, Holland JP, Sprinkle SR, May C, Lewis JS, Scheinberg DA, McDevitt MR. Imaging and treating tumor vasculature with targeted radiolabeled carbon nanotubes. Int J Nanomedicine. 2010; 5:783–802. [PubMed: 21042424]

215. Key J, Leary JF. Nanoparticles for multimodal in vivo imaging in nanomedicine. Int J Nanomedicine. 2014; 9:711–726. [PubMed: 24511229]

216. Luo S, Zhang E, Su Y, Cheng T, Shi C. A review of NIR dyes in cancer targeting and imaging. Biomaterials. 2011; 32:7127–7138. [PubMed: 21724249]

217. Leimgruber A, Berger C, Cortez-Retamozo V, Etzrodt M, Figueirdo JL, Kohler RH, Elpek N, Mempel TR, Swirski FK, Nahrendorf M, Weissleder R, Pittet MJ. Behavior of Endogenous Tumor-Associated Macrophages Assessed In Vivo Using a Functionalized Nanoparticle. Neoplasia. 2009; 11:459–468. [PubMed: 19412430]

218. Yang K, Zhao C, Cao YA, Tang H, Bai YL, Huang H, Zhao CR, Chen R, Zhao D. In vivo and in situ imaging of head and neck squamous cell carcinoma using near-infrared fluorescent quantum dot probes conjugated with epidermal growth factor receptor monoclonal antibodies in mice. Oncology reports. 2012; 27:1925–1931. [PubMed: 22378320]

219. Hellebust A, Richards-Kortum R. Advances in molecular imaging: targeted optical contrast agents for cancer diagnostics. Nanomedicine (Lond). 2012; 7:429–445. [PubMed: 22385200]

220. Skrabalak SE, Chen J, Au L, Lu X, Li X, Xia Y. Gold Nanocages for Biomedical Applications. Adv Mater. 2007; 19:3177–3184. [PubMed: 18648528]

221. Skrabalak SE, Chen J, Sun Y, Lu X, Au L, Cobley CM, Xia Y. Gold Nanocages: Synthesis, Properties, and Applicatiosn. Accounts of Chemical Research. 2008; 41:1587–1595. [PubMed: 18570442]

222. Kircher MF, de la Zerda A, Jokerst JV, Zavaleta CL, Kempen PJ, Mittra E, Pitter K, Huang R, Campos C, Habte F, Sinclair R, Brennan CW, Mellinghoff IK, Holland EC, Gambhir SS. A brain tumor molecular imaging strategy using a new triple-modality MRI-photoacoustic-Raman nanoparticle. Nat Med. 2012; 18:829–834. [PubMed: 22504484]

223. Petersen AL, Hansen AE, Gabizon A, Andresen TL. Liposome imaging agents in personalized medicine. Adv Drug Deliv Rev. 2012; 64:1417–1435. [PubMed: 22982406]

224. Moding EJ, Clark DP, Qi Y, Li Y, Ma Y, Ghaghada K, Johnson GA, Kirsch DG, Badea CT. Dual-energy micro-computed tomography imaging of radiation-induced vascular changes in primary mouse sarcomas. Int J Radiat Oncol Biol Phys. 2013; 85:1353–1359. [PubMed: 23122984]

225. Clark DP, Ghaghada K, Moding EJ, Kirsch DG, Badea CT. In vivo characterization of tumor vasculature using iodine and gold nanoparticles and dual energy micro-CT. Phys Med Biol. 2013; 58:1683–1704. [PubMed: 23422321]

226. Deng L, Ke X, He Z, Yang D, Gong H, Zhang Y, Jing X, Yao J, Chen J. A MSLN-targeted multifunctional nanoimmunoliposome for MRI and targeting therapy in pancreatic cancer. Int J Nanomedicine. 2012; 7:5053–5065. [PubMed: 23028227]

227. Das M, Mishra D, Dhak P, Gupta S, Maiti TK, Basak A, Pramanik P. Biofunctionalized, phosphonate-grafted, ultrasmall iron oxide nanoparticles for combined targeted cancer therapy and multimodal imaging. Small. 2009; 5:2883–2893. [PubMed: 19856326]

228. Lo ST, Kumar A, Hsieh JT, Sun X. Dendrimer nanoscaffolds for potential theranostics of prostate cancer with a focus on radiochemistry. Mol Pharm. 2013; 10:793–812. [PubMed: 23294202]

229. Santra S, Kaittanis C, Grimm J, Perez JM. Drug/dye-loaded, multifunctional iron oxide nanoparticles for combined targeted cancer therapy and dual optical/magnetic resonance imaging. Small. 2009; 5:1862–1868. [PubMed: 19384879]

230. Gautier J, Allard-Vannier E, Munnier E, Souce M, Chourpa I. Recent advances in theranostic nanocarriers of doxorubicin based on iron oxide and gold nanoparticles. J Control Release. 2013; 169:48–61. [PubMed: 23567046]

231. Lee GY, Qian WP, Wang L, Wang YA, Staley CA, Satpathy M, Nie S, Mao H, Yang L. Theranostic nanoparticles with controlled release of gemcitabine for targeted therapy and MRI of pancreatic cancer. ACS Nano. 2013; 7:2078–2089. [PubMed: 23402593]

232. Agemy L, Sugahara KN, Kotamraju VR, Gujraty K, Girard OM, Kono Y, Mattrey RF, Park JH, Sailor MJ, Jimenez AI, Cativiela C, Zanuy D, Sayago FJ, Aleman C, Nussinov R, Ruoslahti E. Nanoparticle-induced vascular blockade in human prostate cancer. Blood. 2010; 116:2847–2856. [PubMed: 20587786]

233. Kenny GD, Kamaly N, Kalber TL, Brody LP, Sahuri M, Shamsaei E, Miller AD, Bell JD. Novel multifunctional nanoparticle mediates siRNA tumour delivery, visualisation and therapeutic tumour reduction in vivo. J Control Release. 2011; 149:111–116. [PubMed: 20888381]

234. Gianella A, Jarzyna PA, Mani V, Ramachandran S, Calcagno C, Tang J, Kann B, Dijk WJ, Thijssen VL, Griffioen AW, Storm G, Fayad ZA, Mulder WJ. Multifunctional nanoemulsion platform for imaging guided therapy evaluated in experimental cancer. ACS Nano. 2011; 5:4422–4433. [PubMed: 21557611]

235. Chen Z, Penet MF, Nimmagadda S, Li C, Banerjee SR, Winnard PT Jr, Artemov D, Glunde K, Pomper MG, Bhujwalla ZM. PSMA-targeted theranostic nanoplex for prostate cancer therapy. ACS Nano. 2012; 6:7752–7762. [PubMed: 22866897]

236. Kao HW, Lin YY, Chen CC, Chi KH, Tien DC, Hsia CC, Lin MH, Wang HE. Evaluation of EGFR-targeted radioimmuno-gold-nanoparticles as a theranostic agent in a tumor animal model. Bioorg Med Chem Lett. 2013; 23:3180–3185. [PubMed: 23628334]

237. Li Z, Jin Q, Huang C, Dasa S, Chen L, Yap LP, Liu S, Cai H, Park R, Conti PS. Trackable and Targeted Phage as Positron Emission Tomography (PET) Agent for Cancer Imaging. Theranostics. 2011; 1:371–380. [PubMed: 22211143]

238. Cheng Z, Al Zaki A, Hui JZ, Muzykantov VR, Tsourkas A. Multifunctional nanoparticles: cost versus benefit of adding targeting and imaging capabilities. Science. 2012; 338:903–910. [PubMed: 23161990]

239. Chen W, Bardhan R, Bartels M, Perez-Torres C, Pautler RG, Halas NJ, Joshi A. A molecularly targeted theranostic probe for ovarian cancer. Mol Cancer Ther. 2010; 9:1028–1038. [PubMed: 20371708]

240. Yang HW, Liu HL, Li ML, Hsi IW, Fan CT, Huang CY, Lu YJ, Hua MY, Chou HY, Liaw JW, Ma CC, Wei KC. Magnetic gold-nanorod/ PNIPAAmMA nanoparticles for dual magnetic

resonance and photoacoustic imaging and targeted photothermal therapy. Biomaterials. 2013; 34:5651–5660. [PubMed: 23602366]

241. Yue C, Liu P, Zheng M, Zhao P, Wang Y, Ma Y, Cai L. IR-780 dye loaded tumor targeting theranostic nanoparticles for NIR imaging and photothermal therapy. Biomaterials. 2013; 34:6853–6861. [PubMed: 23777910]
242. Benachour H, Seve A, Bastogne T, Frochot C, Vanderesse R, Jasniewski J, Miladi I, Billotey C, Tillement O, Lux F, Barberi-Heyob M. Multifunctional Peptide-conjugated hybrid silica nanoparticles for photodynamic therapy and MRI. Theranostics. 2012; 2:889–904. [PubMed: 23082101]
243. Shi J, Yu X, Wang L, Liu Y, Gao J, Zhang J, Ma R, Liu R, Zhang Z. PEGylated fullerene/iron oxide nanocomposites for photodynamic therapy, targeted drug delivery and MR imaging. Biomaterials. 2013; 34:9666–9677. [PubMed: 24034498]
244. Yang L, Sajja HK, Cao Z, Qian W, Bender L, Marcus AI, Lipowska M, Wood WC, Wang YA. uPAR-targeted optical imaging contrasts as theranostic agents for tumor margin detection. Theranostics. 2013; 4:106–118. [PubMed: 24396518]
245. Agdeppa ED, Spilker ME. A Review of Imaging Agent Developmen. The AAPS Journal. 2009; 2:286–299. [PubMed: 19415506]
246. Nunn AD. The Cost of Developing Imaging Agents for Routine Clinical Use. Investigative Radiology. 2006; 41:206–212. [PubMed: 16481902]
247. Gorovets A, Marzella L, Rieves D, Yang L. Efficacy considerations for U.S. Food and Drug Administration approval of diagnostic radiopharmaceuticals. J Nucl Med. 2013; 54:1479–1484. [PubMed: 23749997]
248. Farrell D, Ptak K, Panaro NJ, Grodzinski P. Nanotechnology-based cancer therapeutics--promise and challenge--lessons learned through the NCI Alliance for Nanotechnology in Cancer. Pharm Res. 2011; 28:273–278. [PubMed: 20814720]
249. Zamboni WC, Torchilin V, Patri AK, Hrkach J, Stern S, Lee R, Nel A, Panaro NJ, Grodzinski P. Best practices in cancer nanotechnology: perspective from NCI nanotechnology alliance. Clin Cancer Res. 2012; 18:3229–3241. [PubMed: 22669131]
250. Szebeni J, Muggia F, Gabizon A, Barenholz Y. Activation of complement by therapeutic liposomes and other lipid excipient-based therapeutic products: prediction and prevention. Adv Drug Deliv Rev. 2011; 63:1020–1030. [PubMed: 21787819]

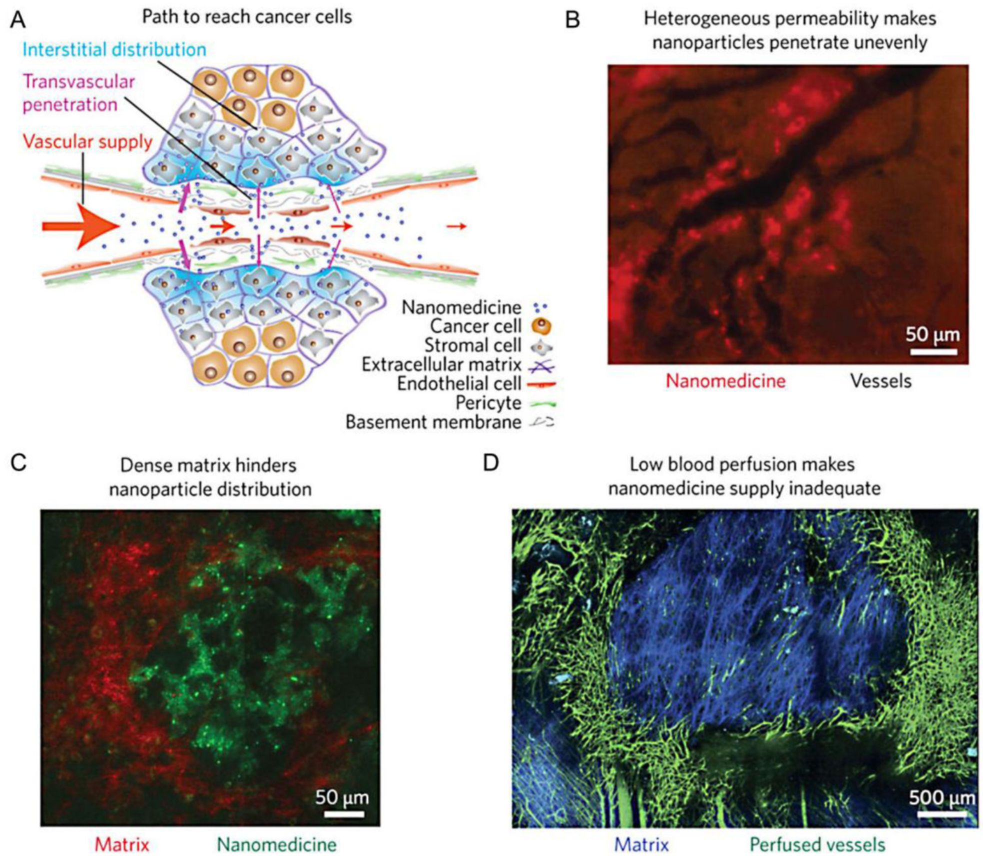

Fig. 1. Challenges for delivering nanoparticles to tumor tissues

(A) In healthy blood vessels, the vascular endothelium is continuous and supported by pericytes, which is impermeable to nanoparticles. In angiogenic tumor blood vessels, the endothelial wall is not fully formed. As a result, nanoparticles have the ability to extravasate and enter the tumor interstitial space. (B) Rapid tumor angiogenesis results in heterogeneous blood vessel development, which results in variable vascular permeability and leads to uneven nanoparticle distribution. (C) Furthermore, the dense extracellular matrix inside the tumor prevents nanoparticles from traveling far away from its blood vessel of origin. (D) Overall, blood perfusion is low inside a tumor, which often limits nanoparticle deposition to the tumor periphery. **Reproduced with permission from reference** [35].

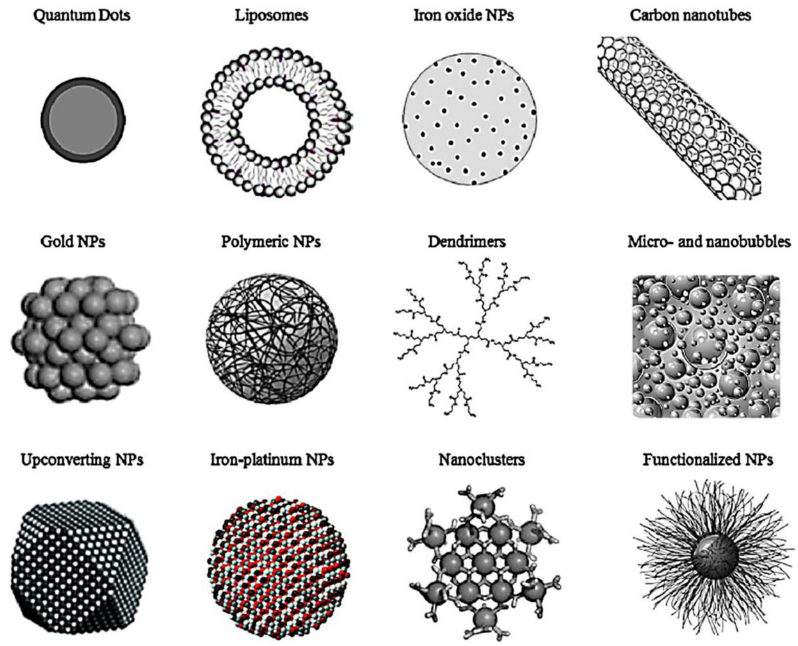

Fig. 2. Common nanoparticle platforms for medical imaging

Contrast agents may be developed as discrete crystalline geometries (spheres, rods, cubes, etc.), or incorporated into a variety of nanoparticle platforms, such as being entrapped in dendrimers, liposomes or micelles, or loaded into capsules, such as porous silica nanoparticles.

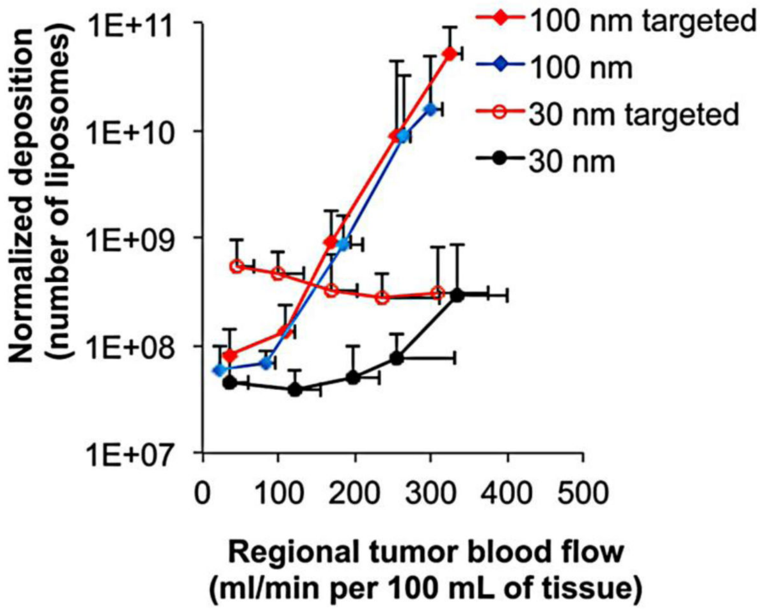

Fig. 3. Blood flow effects on the interstitial deposition of nanoparticles

Following tumor blood flow mapping using perfusion CT, the intratumoral deposition of four different liposome classes (30 and 100 nm with or without EGFR-targeting ligands) was quantitatively measured in the orthotopic mouse (4T1) mammary tumor using Fluorescence Molecular Tomography imaging at 24 h after injection. To image all four liposome classes in the same tumors, distinct NIR fluorophores were used to distinguish each class of liposome inside the tumor. The intratumoral deposition of liposomes is shown as a function of regional blood flow in tumors, which indicates that a large nanoparticle's transport is heavily governed by convection. For nanoparticles in this size regime, high blood flow is essential for nanoparticle retention inside the tumor. On the other hand, while convection is the primary mode of transport, the diffusion of small nanoparticles contributes to their transport. In the absence of convection, smaller nanoparticles have the ability to move both in and out of a tumor. For smaller nanoparticles, active targeting to cellular receptors deep in the tumor interstitium prevents the return of nanoparticles back into the bloodstream. **Reproduced with permission from reference** [30].

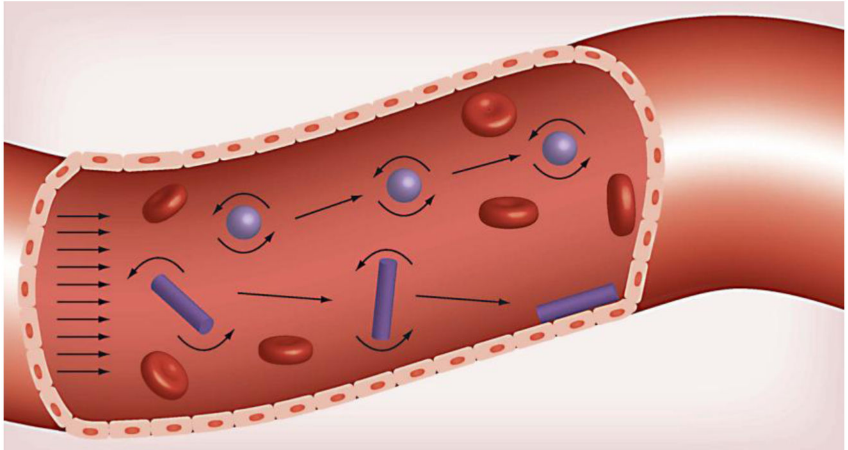

Fig. 4. Designing nanoparticles for enhanced margination

The symmetry of a spherical nanoparticle results in its tendency to remain in the blood flow. Variable drag forces and torques which act on an oblate shaped nanoparticle, however, enable oscillatory movement within a blood vessel that increases meaningful interactions with the blood vessel wall. **Reproduced with permission from reference** [38].

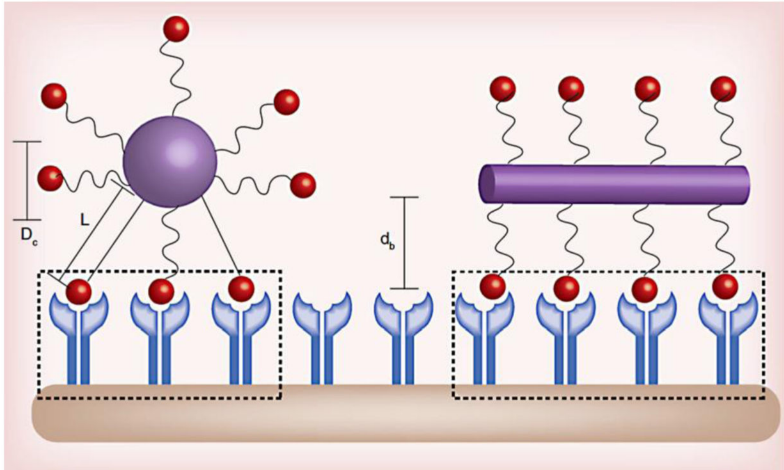

Fig. 5. Effect of shape on nanoparticle binding avidity

Shape, ligand length, and polymer flexibility all play a role in the active fractional area of a nano-carrier (AFAC). For a sphere, the AFAC is defined as $(L\text{-}d_B)/D_c$, where L is the length of the ligand, db is the binding distance between the nanoparticle and the receptor, and ^{D}c is the diameter of the nano-carrier. For particles with equal surface area, the ligand length, binding distance, and shape affects AFAC. **Reproduced with permission from reference** [38].

NIH-PA Author Manuscript

NIH-PA Author Manuscript

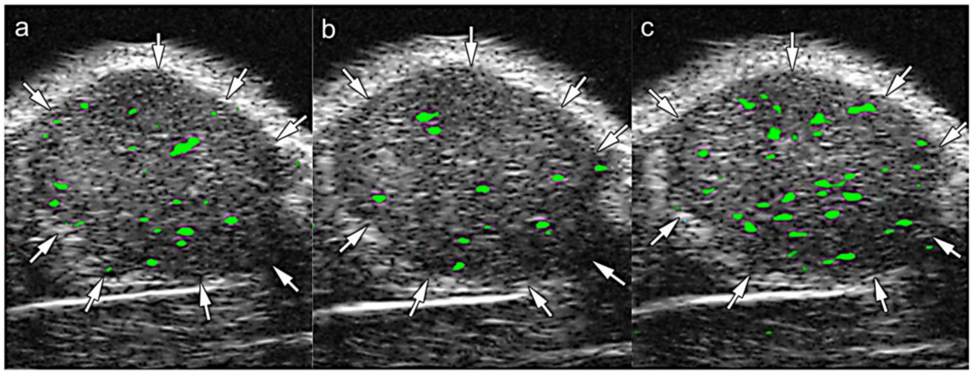

Fig. 6. Dual targeting improves the efficacy of contrast-enhanced ultrasound with targeted microbubbles

Transverse color-coded ultrasound images demonstrating imaging of tumor angiogenesis in a mouse model of subcutaneous human ovarian adenocarcinoma (SKOV-3) xenograft tumor. Images were acquired in the same imaging session 4 minutes after IV injection of (a) anti-VEGFR2-targeted microbubbles, (b) anti-$\alpha_v\beta_3$-integrin-targeted microbubbles, and (C) microbubbles targeted to both VEGFR2 and $\alpha_v\beta_3$ integrin. Injections were spaced out in 30 minute intervals to allow time for clearance of the previous microbubble formulation. Difference in video intensity (color-coded as green signal from adherent microbubbles on greyscale ultrasound images) was highest after administration of the dual-targeted particle. **Reproduced with permission from [**109].

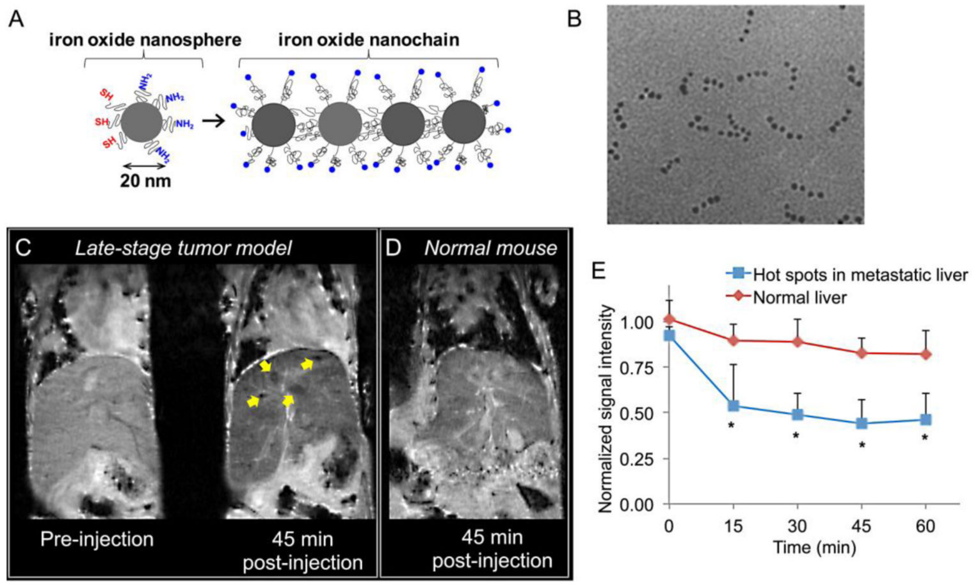

Fig. 7. Detection of breast cancer metastasis in liver using MRI and a targeted iron oxide nanochain

(A) Illustration of the RGD-targeted nanochain nanoparticle and its constituent iron oxide nanospheres. (B) TEM image of the nanochain particles predominantly composed of four IO spheres. (C) Representative *in vivo* MR images of the liver in normal and metastasis-bearing mice were obtained using a 9.4 T MRI. Coronal *T*2-weighted images of the liver of a metastatic mouse before and 45 min after injection of the RGD-targeted nanochains. In the 45 min post-injection image, the yellow arrows show micrometastases of about 0.5 mm in size with increased contrast enhancement. (D) Coronal *T*2-weighted images of the liver of a normal mouse 45 min after injection of the nanochains. (E) Time course of the MR signal intensity in the liver hot spots was quantitatively evaluated. The absolute MR signal intensity in the metastatic lesions and the healthy liver was measured in manually drawn ROIs. The signal intensity in the hot spots or the entire healthy liver was normalized to the signal of an adjacent muscle (scale: 0–1). Since lower values indicate greater contrast in *T*2 images, normalized intensity values of 0 and 1 correspond to maximum and minimum contrast, respectively, compared to the precontrast intensity values (data presented as mean ± standard deviation; n=3; each metastatic animal exhibited 2–4 hot spots; *P< 0.05). **Reproduced with permission from reference** [56]

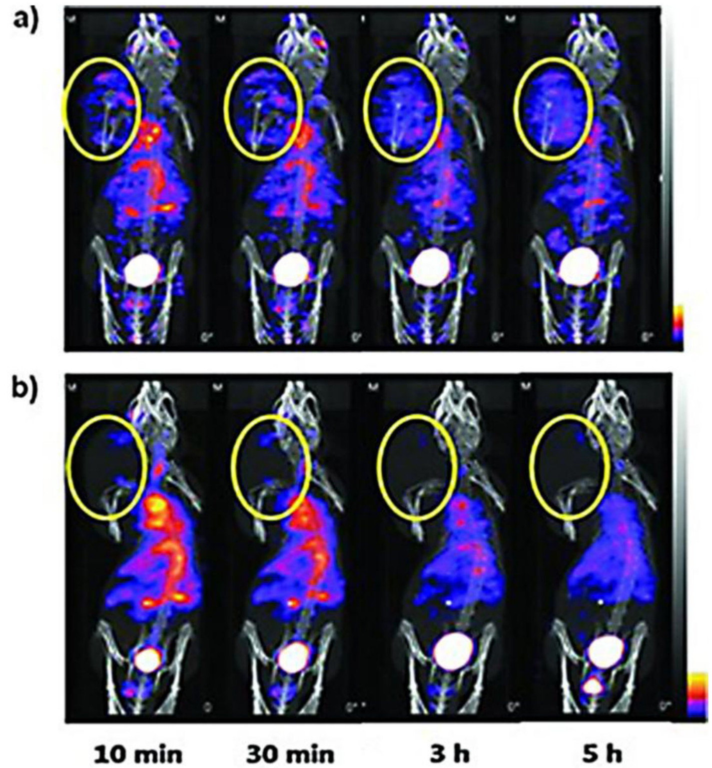

Fig. 8. Tumor targeting and imaging using cyclic RGD-targeted PEGylated gold nanoparticle probes with directly conjugated iodine-125

(A) Small animal SPECT/CT of ^{125}I-cRP-AuNPs and (B) cold-form-blocked ^{125}I-cRGD-AuNP in nude mice with U87MG brain tumor xenografts. Imaging was performed serially from 0 to 5 h after IV injection of 11.1 MBq radiolabeled AuNP. Tumor ROIs are designated in yellow circles.

(Adapted with permission from) [131].

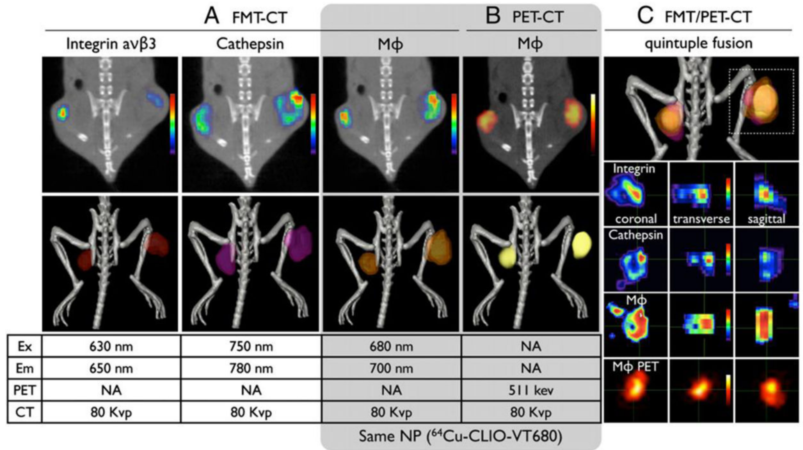

Fig. 9. Multimodal imaging with hybrid PET-optical dextran nanoparticle enables visualization of tumor biomarker expression

In vivo multichannel FMT/PET-CT of tumor-bearing mice, co-injected with a fluorophore-derived RGD peptide that targets integrin, a fluorescent sensor that targets cathepsins, and a nanoparticle PET agent (^{64}Cu-CLIO-VT-680). In 2D images, (A) FMT and (B) PET, signal intensities were color-coded and 3D images show a surface-rendered image. (C) The signals in FMT channels and in PET co-localized in tumors, but distinct differences between the expression of each probe was observed at higher magnification. **Reproduced with permission from reference** [207].

Table 1

Effect of nanoparticle design on pharmacokinetics, margination, and binding avidity

Design parameter	Pharmacokinetics	Margination	Binding Avidity
Size	Small particles (<10 nm) are cleared renally, larger particles are cleared by liver and spleen [42–45]	More difficult for larger particles to escape the blood flow [39]	Larger particles preferred increased # of binding interactions [46–48]
Shape	Oblate shapes preferred – more difficult to internalize by macrophages [49–51]	Oblate shapes preferred – higher margination due to variable torques and drag forces [52–56]	Oblate and discoidal shapes offer higher numbers of surface ligands available for interactions with receptor bed [57, 58]
Surface chemistry	Appropriate polymeric coating extends blood circulation [59]	The length of the polymeric coating influences the hydrodynamic size [59]	Optimum # of ligands maximizes binding avidity [59–61]

Table 2

Summary of nanoparticle platforms utilized for development of targeted imaging agents

Imaging Modality	Nanoparticle Platform	Ligand Type	Target	Reference
Computed Tomography	Gold Nanospheres	Antibody	Her2	[93]
			CD4	[94]
			EGFR	[95]
		Peptide	GRP receptor	[96]
		Aptamer	PSMA	[97]
	Gold Nanorods	Antibody	A9 Antigen	[98]
	Dendrimer (gold)	Small molecule	FA Receptor	[99]
			Thrombus	[100]
	Bismuth Nanoparticles	Protein	Thrombus	[101]
Ultrasound	Microbubbles	Peptide	Integrin	[102–107]
			VEGF/KDR	[108]
		Antibody	Integrin	[103]
			Integrin/VEGF	[109]
MRI	Iron Oxide Nanochains	Peptide	Integrin	[56]
	Iron Oxide Nanoparticles	Peptide	Integrin	[110]
			uPA Receptor	[111]
			EDB	[112]
		Antibody	Chemokine Receptor	[113]
			VEGF	[114]
		Protein	Transferrin Receptor	[115]
	Capsules (iron oxide)	Peptide	Integrin	[116]
	Lipid-based (gadolinium)	Peptide	Integrin	[117, 118]
			Integrin/galectin-1	[119, 120]
		Antibody	ICAM-1	[121]
			CD105	[122]
		Small molecule	FA Receptor	[123]
	Perfluorocarbon Nanoparticles	Various	Various	[124]
		Peptide	Integrin	[125]
		Antibody	Integrin	[126]

NIH-PA Author Manuscript
NIH-PA Author Manuscript

Imaging Modality	Nanoparticle Platform	Ligand Type	Target	Reference
	LipoCEST	Peptide	Integrin	[127]
	Dendrimers (Gd)	Small molecule	FA Receptor	[128, 129]
Nuclear Imaging	Gold Nanoparticles (^{64}Cu)	Peptide	Integrin	[130]
	Gold Nanoparticles (^{125}I)	Peptide	Integrin	[131]
	Silica Nanospheres ^{64}Cu)	Antibody	CD105	[132]
	Lipid-based (^{111}In)		Integrin	[133]
Optical Imaging	Gold Nanoparticles	Antibody	EGFR	[134–136]
	Gold Nanoshells	Antibody	Her2	[137, 138]
	Gold Nanorods	Antibody	EGFR	[139–141]
	Rare-Earth Nanocrystals	Small molecule	FA Receptor	[142]
	NIR Dye Encapsulation	Antibody	Her2	[143]
	Dendrimers (NIR dye)	Peptides	MMPs	[144]
	NIR-labeled Iron Oxide Nanoparticle	Antibody	Her2	[145]
	Quantum Dots	Peptide	Integrin	[146]
		Antibody	EGFR	[147, 148]
Multimodal Imaging	SPECT-MRI	Peptide	Integrin	[149]
	PET-MR	Peptide	Integrin	[133]
	Optical MR	Peptide	CPP	[144]